The deep Arctic Ocean and Fram Strait in CMIP6 models

Céline Heuzé,[a] Hannah Zanowski,[b] Salar Karam,[a] and Morven Muilwijk[c]

[a] *Department of Earth Sciences, University of Gothenburg, Gothenburg, Sweden*

[b] *Department of Atmospheric and Oceanic Sciences, University of Wisconsin-Madison, Madison, US*

[c] *Norwegian Polar Institute, Tromsø, Norway*

The deep Arctic Ocean and Fram Strait in CMIP6 models

Céline Heuzé,[a] Hannah Zanowski, [b] Salar Karam, [a] and Morven Muilwijk[c]

[a] *Department of Earth Sciences, University of Gothenburg, Gothenburg, Sweden*

[b] *Department of Atmospheric and Oceanic Sciences, University of Wisconsin-Madison, Madison, US*

[c] *Norwegian Polar Institute, Tromsø, Norway*

Corresponding author: Céline Heuzé, celine.heuze@gu.se

ABSTRACT: Arctic sea ice loss has become a symbol of ongoing climate change, yet climate models still struggle to reproduce it accurately, let alone predict it. A reason for this is the increasingly clear role of the ocean, especially the "Atlantic layer", on sea ice processes. We here quantify biases in that Atlantic layer and the Arctic Ocean deeper layers in 14 representative models that participated in the Climate Model Intercomparison Project phase 6. Compared to observational climatologies and a database of hydrographic profiles, the modelled Atlantic layer core is too cold by on average -0.4°C and too deep by 400 m in the Nansen basin, in too thick a layer that, in some models, extends to the seafloor. Deep and bottom waters are in contrast too warm by 1.1 and 1.2°C. Furthermore, the properties hardly change throughout the Arctic. We attribute these biases to an inaccurate representation of shelf processes: only three models seem to produce dense water overflows, at too few locations, and these do not sink deep enough. No model compensates with open ocean deep convection. Therefore, the properties are set by the inaccurate fluxes through Fram Strait, biased low by up to 6 Sv, but coupled to a too-warm Fram Strait, resulting in a somewhat accurate heat inflow. These fluxes are related to biases in the Nordic Seas, themselves previously attributed to inaccurate sea ice extent and atmospheric modes of variability, thus highlighting the need for overall improvements in the different model components and their coupling.

SIGNIFICANCE STATEMENT: Coupled climate models are routinely used for climate change projection and adaptation, but they are only so good as the data used to create them. And in the deep Arctic, those data are few. We determine how biased 14 of the most recent models are regarding the deep Arctic Ocean and the Arctic's only deep gateway, Fram Strait (between Greenland and Svalbard). They are very biased: too cold where they should be warm, too warm where they should be cold, not stratified enough, not in contact with the surface as they should, moving the wrong way around the Arctic, etc. The problem seems to come from out of the Arctic and/or out of the ocean.

1. Introduction

The Arctic is one of the regions most affected by ongoing climate change (IPCC 2019), warming 2–3 times as fast as the global average (IPCC 2021) and consequently losing its sea ice cover. Since the beginning of the satellite record, the sea ice extent has been reduced by more than 1 m^2 per year per ton CO_2 in winter, and more than 3 m^2 per year per ton CO_2 in summer (Stroeve and Notz 2018), while the sea ice thickness has been reduced by 66% (Kwok 2018). The multi-year ice area has halved (Kwok 2018), and as a result the shelves have become seasonally ice free (Onarheim et al. 2018). These changes are associated with changes in freshwater content in the upper ocean (Solomon et al. 2021, and references therein), but more and more clearly seem to be caused by and enhancing changes in the deeper layers (Årthun and Eldevik 2016), in particular the Atlantic Water, via a process known as the "Atlantification" of the Arctic Ocean (Polyakov et al. 2017). Climate models, however, fail to reproduce the sea ice evolution (Notz and SIMIP Community 2020), notably because their upper Arctic Ocean representation strongly varies among models (Ilıcak et al. 2016; Lique and Thomas 2018; Zanowski et al. 2021). We here investigate their representation of the deeper Arctic ocean layers, from the Atlantic Water to the seafloor.

The Arctic Ocean consists of four deep basins (Fig. 1): the Nansen and Amundsen basins on the Eurasian side, and the Makarov and Canada basins on the Amerasian side, separated by the Lomonosov Ridge. The Eurasian basin contains two water masses below 1000 m (Smethie et al. 1988): the Eurasian Basin Deep Water (EBDW, down to 2500 m depth) and Eurasian Basin Bottom Water (EBBW, from 2500 m to the seafloor). The denser deep and bottom waters are primarily the result of sea ice formation on the Siberian shelf (Nansen, F. 1906): when sea ice forms, brine is rejected, and the resulting dense water cascades off the shelf through troughs and canyons (Aagaard 1981; Rudels et al. 1999). This cascading is often referred to as "overflow", the term we use in this manuscript. The only deep connection between the Arctic Ocean and the global oceanic circulation is via Fram Strait (ca 2500 m deep), through which the comparatively warm and salty Atlantic Water enters from the Nordic Seas. North of Fram Strait, the Atlantic Water circulates cyclonically around the entire Arctic Ocean at depths no greater than 900 m (Rudels et al. 1999; Aksenov et al. 2011). However, its properties impact the whole water column as it can be entrained by the overflows (Smethie et al. 1988; Frank et al. 1998; Valk et al. 2020). At the bottom of Fram Strait, the Eurasian Basin Deep Water flows out. Part of it mixes with fresh Greenland Sea deep waters and flows back into the Arctic through Fram Strait (Frank et al. 1998; Langehaug and Falck 2012; von Appen et al. 2015), below the Atlantic Water. In the Amerasian basin, the deep water mass is the Canada Basin Deep Water (CBDW), the saltiest and warmest of the Arctic deep waters (Aagaard et al. 1985), suspected to be modified Eurasian Basin Deep Water that intruded through the Lomonosov Ridge. There is no agreement as to whether this intrusion happens continuously (Timmermans and Garrett 2006), in pulses (Timmermans et al. 2005), or whether it happened and stopped centuries ago (Schlosser et al. 1997). The higher salinity and temperature of this Canada basin deep water compared to its Eurasian source is most likely caused by shelf overflows in the Amerasian basin (Rudels 1986; Ivanov et al. 2004). Eventually, Canada Basin Deep Water intrudes back into the Eurasian basin through canyons in the Lomonosov Ridge (orange arrows on Fig. 1), as a very salty deep water (Björk et al. 2018).

To properly represent the deep Arctic circulation, models need to accurately simulate 1. sea ice and upper Arctic Ocean processes, 2. flow through Fram Strait and upstream ocean properties, and 3. bathymetry. Earlier studies suggest that this was challenging in the previous generation of climate models (Shu et al. 2019) and will continue to be challenging for the models that participated in the latest Climate Model Intercomparison Project, phase 6 (CMIP6, Eyring et al. 2016): their Arctic sea ice (Notz and SIMIP Community 2020), Arctic solid and liquid freshwater storage and fluxes (Zanowski et al. 2021), and properties and processes upstream in the Nordic Seas (Heuzé 2021) are inaccurate, or at least the models have a large range of behaviours. The vast majority also fail to reproduce overflows in other parts of the world (Heuzé 2021). Khosravi et al. (2022) recently published an overview of biases in the Atlantic Water; we here expand on their results

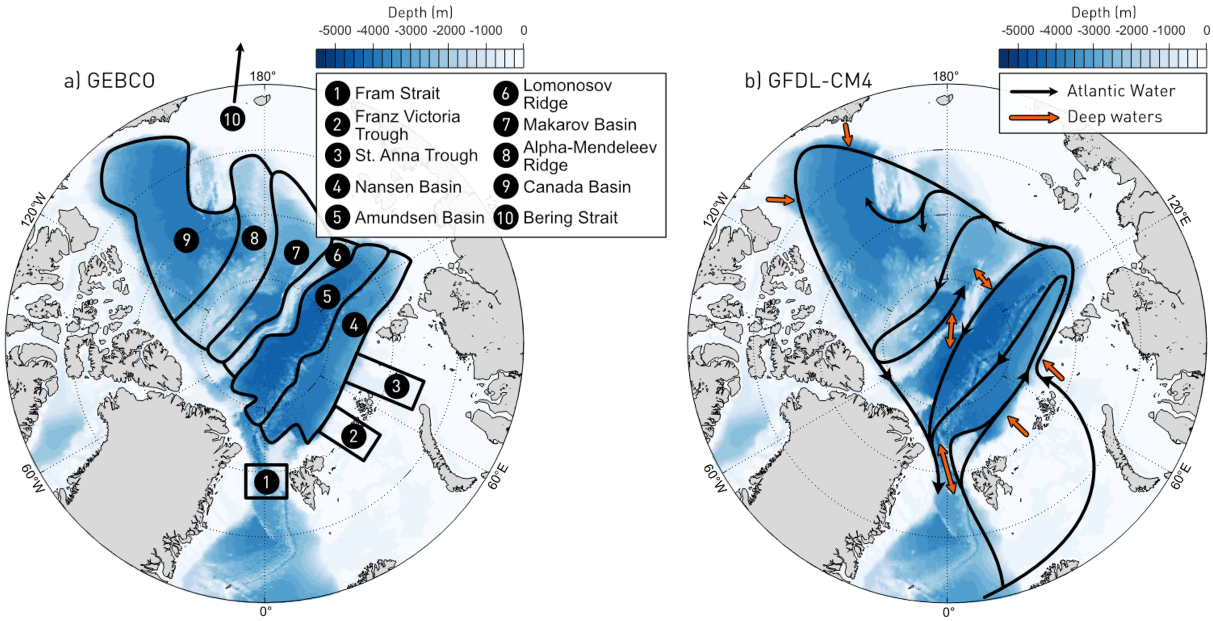

Fig. 1. Bathymetry of the Arctic north of 70 °N in a) GEBCO (GEBCO Compilation Group 2021) and b) the CMIP6 model with the highest resolution in our study, GFDL-CM4 (Adcroft et al. 2019). Contours and numbers on a) highlight the regions discussed in this manuscript. Black arrows on b) indicate the known circulation of the Atlantic layer (e.g. Rudels 2009); orange arrows, the main features of the deep water circulation.

by assessing not only the Atlantic Water but also the deep and bottom waters, and by explaining the causes for all these biases, focussing on the models' mean historical state only. We start by describing the 14 CMIP6 models and methods that we use (Section 2) before quantifying the biases in all Arctic deep waters in all basins (Section 3a). We then assess the representation of overflows and circulation of the deep water masses within the Arctic (Section 3b) and finally evaluate the fluxes through Fram Strait and their relation to the biases in the Arctic (Section 3c). We finish with a discussion, notably on possible directions for CMIP7 (Section 4).

2. Data and Methods

a. The CMIP6 models

We use the output from 14 fully coupled models that participated in the Climate Model Intercomparison Project phase 6 (CMIP6, Eyring et al. 2016), listed in Table 1. These models were selected following a preliminary study on the 35 CMIP6 models used in Heuzé (2021) as representative of

Table 1. Characteristics of the 14 CMIP6 models used in this study: horizontal grid type, which output if any are missing, horizontal resolution in the Arctic, type of vertical grid and number of vertical levels, ocean model component, ocean climatology used to initialise the model, and reference. The horizontal resolution in the Arctic (4th column) was calculated as the square root of the total area north of 70°N divided by the number of points the model has north of 70°N. For the vertical grids, ρ means isopycnic; σ terrain-following; and several symbols, hybrid.

Model	Grid type	Missing	Resolution	Vertical grid	Ocean model	Initialisation	Reference
BCC-CSM2-MR	Tripolar	agessc	54 km	z 40	MOM4-L40v2	WOA13	Wu et al. (2019)
CAMS-CSM1-0	Tripolar	agessc	54 km	z 50	MOM4	WOA2001	Rong et al. (2019)
CESM2	Rotated	/	41 km	z 60	POP2	PHC2(.0?)	Danabasoglu et al. (2020)
CanESM5	Tripolar	/	50 km	z 45	NEMO3.4.1	WOA09	Swart et al. (2019)
EC-Earth3	Tripolar	agessc	49 km	z* 75	NEMO3.6	WOA13	Döscher et al. (2021)
GFDL-CM4	Tripolar	agessc	9 km	ρ-z* 75	MOM6	WOA13	Adcroft et al. (2019)
GFDL-ESM4	Tripolar	agescc, uo, vo	18 km	ρ-z* 75	MOM6	WOA13	Dunne et al. (2020)
GISS-E2-1-H	Regular	agessc	46 km	ρ-z-σ 32	Hycom	WOA13	Kelley et al. (2020)
IPSL-CM6A-LR	Tripolar	/	49 km	z* 75	NEMO3.2	WOA13	Lurton et al. (2020)
MIROC6	Tripolar	/	39 km	z-σ 62	COCO4.9	PHC3	Tatebe et al. (2019)
MPI-ESM1-2-HR	Tripolar	/	36 km	z 40	MPIOM1.63	PHC3	Müller et al. (2018)
MRI-ESM2-0	Tripolar	/	39 km	z* 60	MRI.COMv4	WOA13	Yukimoto et al. (2019)
NorESM2-LM	Tripolar	/	38 km	ρ-z 53	BLOM (MICOM)	PHC3	Seland et al. (2020)
UKESM1-0-LL	Tripolar	/	50 km	z* 75	NEMO3.6	EN4(.2.1?)	Sellar et al. (2020)

their family, for diversity in vertical grid types, for comparison with those used in a companion paper (Muilwijk et al. subm.), and after eliminating the ones with the lowest resolution or poorest bathymetry. Most of the models we selected have a resolution of ~50 km in the Arctic (9 km for the highest resolution) and 50 levels or more in the vertical. No more than two models share the same ocean component with the same version, and these 14 models have been initialised using 6 different ocean climatologies (Table 1).

We evaluate the last 30 years of the historical run, i.e. January 1985 - December 2014, and only one ensemble member for each model. The output we use are the monthly seawater salinity 'so', potential temperature 'thetao', eastward velocity 'uo', and northward velocity 'vo', except for GFDL-ESM4 for which uo and vo were not archived. For 8 models, we also use the seawater age since surface contact 'agescc', which we will hereafter refer to as the age of water. For the mixed layer depth, we used the 'mlotst' output when available, and otherwise computed it as per the CMIP6 protocol by first computing the potential density σ_θ from the monthly salinity and temperature, and then using a threshold of 0.125 kg m^{-3} referenced to 10 m depth. The 'mlotst' and computed values are not the same due to the non-linearity of the equation of state, but as shown in Heuzé (2021), the difference is not significant for shallow mixed layers. With the exception of the mixed layer computation, we use the density referenced to 2000 m depth σ_2 as a compromise considering the wide range of depths covered. The diagnostics based on σ_2 differences were also done using σ_0 and σ_4 (not shown), but no significant differences in our results were found. All densities were computed using the TEOS10 equation of state as implemented in the Gibbs-SeaWater (GSW) Oceanographic Toolbox (McDougall and Barker 2011).

All computations were performed on the models' native grid with these two exceptions:

- The GISS-E2-1-H and NorESM2-LM native vertical grids were particularly challenging to work with, so we instead show their regularised grid output. We nevertheless verified that our key results still hold on the native grid;
- The comparisons to the climatology in section 3.a and 3.c were performed after interpolating all the model temperature and salinity values onto the climatology's grid.

b. Observational data

To quantify biases in the CMIP6 models, we first compare them to the Unified Database for Arctic and Subarctic Hydrography (UDASH, Behrendt et al. 2018) by generating basin- 30-year-average temperature and salinity profiles in the four deep basins of the Arctic Ocean (as defined on Fig. 1). As the UDASH profiles are scattered, rather than interpolate them ourselves we use the World Ocean Atlas 2018 (WOA18, Locarnini et al. 2018; Zweng et al. 2018) objectively analysed annual fields at a 0.25° resolution for all computations where the model and observations had to be colocated.

As we will show in this manuscript, the deep waters appear to not be ventilated and can be much older than in observations (e.g. Tanhua et al. 2009). One hypothesis that we test is whether the deep ocean is, in fact, still relaxing from its initialisation. To test this hypothesis, we needed to know the climatology with which the model was initiliased, which is often not indicated in the model description, although several modelling centres did (Danabasoglu et al. 2020; Seland et al. 2020; Tatebe et al. 2019) or even produced a tuning-specific publication (Mignot et al. 2021). For all other models listed in Table 1, we obtained information regarding the climatology after email exchange with the modellers (see Acknowledgments).

Most models use an earlier version of the World Ocean Atlas as initialisation, with 7 out of 14 models using the version that was the latest as the models ran, i.e. WOA13. Two models use an even earlier version from 2009 or even 2001. The main difference between the versions is the amount of data ingested and the time period of the data; the reader will find more information about the versions' differences in the WOA18 publications (Locarnini et al. 2018; Zweng et al. 2018). The second most common climatology is the Polar science center Hydrographic Climatology (PHC, Steele et al. 2001), which includes the WOA98 data and the Arctic Ocean Atlas (AOA, Environmental Working Group 1997, 1998), gridded compilation of previously classified US and Russian hydrographic data collected during the Cold War. One model uses the original PHC2 from 2001, while three models use the updated PHC3 from 2005. Finally, the Met Office Hadley Centre model UKESM1-0-LL uses the Met Office Hadley Centre climatology EN4 (Good et al. 2013), which merges the World Ocean Database 2009 with many available Arctic observations and Argo data (see Good et al. 2013, for more information). All these products have a 1x1° horizontal resolution.

c. Methods

The primary objective of this paper is to quantify biases in the properties of the deep water masses of the Arctic Ocean: the Atlantic Water (AW), the Eurasian Basin Deep Water (EBDW), its counterpart the Canada Basin Deep Water (CBDW), and the Eurasian Basin Bottom Water (EBBW). Traditionally, for observational datasets, the definition of these water masses is based on temperature, salinity, or density values (e.g. Smethie et al. 1988; Rudels 2009; Korhonen et al. 2013). As we expect these properties to be biased in the models, we instead chose these three definitions:

- the Atlantic Water core is the depth of the temperature maximum, between 100 and 2000 m depth. This definition is similar to the real Arctic, but without imposing a constraint on the value of the temperature maximum;

- deep water properties are those at 2000 m. In observations, EBDW sits between approx. 1000 and 2500 m depth in the Eurasian basin, and CBDW extends from approx. 1000 m all the way to the seafloor;

- bottom water properties are those of the deepest grid cell with a value.

The upper ocean is not the topic of this paper. We nevertheless investigate whether biases in the upper ocean and in the deep layers are related, and therefore computed the mean temperature, salinity, and density in the top 100 m as a proxy for upper ocean properties. Similarly, a detailed study of stratification is provided by Muilwijk et al. (subm.); we here only provide a simplified definition of stratification, taken as the difference between the upper 100 m mean density and that of the AW core.

We compare the properties of the different water masses in the four deep basins of the Arctic north of 70°N (Fig. 1a), where "deep" is defined as deeper than 2000 m. The shelf is defined as shallower than 1000 m. Throughout this manuscript, we use the short name "Siberian shelf" to refer to the shelf along the Eurasian basin, i.e. from Fram Strait to 160°W. As we will show, no deep water formation occurs on the shelf along the Canada basin, so we do not focus on this region. Finally, to briefly investigate the deep outflows from the Arctic, we determine the biases on the Greenland shelf, i.e. around Greenland but north of 70°N.

In the Arctic, dense waters cascading from the shelf to the deep basin, commonly referred to as overflows, strongly modify the properties of all water masses (e.g. Aagaard 1981; Luneva et al. 2020). As summarised in Luneva et al. (2020), these overflows are bottom-trapped gravity currents characterised by a comparatively high density, but also by a young age, as they sink off the shelf within the same year that they sank from the surface to the shelf seafloor. Therefore, we detect their presence in models by studying:

- the minimum age at the bottom grid cell, for the 8 models that provided the age of water output

- the maximum bottom density, for the other 6 models.

For both groups of models, we look for a continuity in this diagnostic on and off the shelf, in maps of the bottom properties, and in sections along and across the troughs where we expect their presence.

Finally, we determine the influence of Fram Strait on the deep Arctic Ocean properties by computing the volume, salt, and heat fluxes through that section as follows, where S is the salinity, θ is the potential temperature, ρ_2 is the potential density referenced to 2000 dbar ($\rho_2 = \sigma_2 + 1000$, with σ_2 defined previously), and $c_p = 3900$ J kg^{-1} K^{-1}:

$$F_{volume} = \iint_A \mathbf{v} \cdot \hat{n} dA \quad (1)$$

$$F_{salt} = \iint_A S\mathbf{v} \cdot \hat{n} dA \quad (2)$$

$$F_{heat} = c_p \iint_A \rho_2 \theta \mathbf{v} \cdot \hat{n} dA \quad (3)$$

Note that strictly speaking, this is no true transport as this would require a closed volume budget across Fram Strait (Schauer and Beszczynska-Möller 2009). This method is nevertheless routinely used to compute "volume fluxes" and "heat fluxes" from observations, so we use it to enable comparison between models and the real Arctic and refer to it as fluxes (without quotation marks). Besides, each model's heat flux should in theory be computed relative to a temperature representative of the flow. That is, for each model, the shallow inflow, shallow outflow, deep inflow and deep outflow, if all clearly distinguishable, would each have a different reference temperature. To ease the across-model comparison, all heat fluxes are instead computed relative to 0°C (as done in e.g. Ilıcak et al. 2016; Muilwijk et al. 2018). Similarly, instead of computing a so-called freshwater flux, i.e. relative to a reference salinity which would, again, have to be meaningful for each specific model, we compute the flux of salt. As its value is rarely given in the literature, we focus our analysis on F_{volume} and F_{heat}.

As in Zanowski et al. (2021), the boundaries for Fram Strait were chosen by hand for each model and span 20°W-12°E, 78°N-80°N. For the rotated and tripolar grids, the northward velocity 'vo' does not correspond to velocities towards the true north 90°N but rather towards the model's location of the North Pole. Therefore, for all models, $\mathbf{v} \cdot \hat{n}$ is the velocity into / out of the Arctic, normal to the model's coast-to-coast section. All fluxes were computed on the models' native horizontal grids. CMIP6 variable 'thkcello' (ocean model cell thickness) was used for those models with time-varying cell thicknesses, unless specific instructions were provided in the model output for computing cell thickness (i.e., MIROC6, GFDL-CM4). The routines are freely available on Zenodo (doi:10.5281/zenodo.4606856).

3. Results

In this section, we first quantify the biases in the properties of the Atlantic Water, deep, and bottom water masses and their horizontal and vertical relationships. We then evaluate the representation of the processes that set these properties, within the Arctic Ocean (subsection 3b) and at Fram Strait (subsection 3c).

a. Biases in water mass properties

We start by quantifying biases in the mean temperature and salinity and their evolution with depth in the four deep basins (Fig. 2 and individual values in supp. Tables A1 to A3). As the Nansen basin lies closest to its inflow, in observations, the Atlantic Water, defined as the profile's temperature maximum, is warm (black line, Fig. 2a), salty (Fig. 2b) and constrained to a narrow shallow depth range, around 200 m depth. In the models in contrast (colours), the Atlantic Water lies deeper (multimodel average of 395 m, ranging from 76 to 1321 m) and occupies a thicker layer, which is in agreement with the findings of Khosravi et al. (2022) in CMIP6, and Ilıcak et al. (2016) for CORE-II. In fact, had we used the standard definitions that the Atlantic Water is anything warmer than 0°C (e.g. Korhonen et al. 2013) or lighter than 27.97 kg m^{-3} (e.g. Rudels 2009) (black dotted lines on Fig. 2c), we would have found Atlantic Water all the way to the seafloor in half of the models. Therefore, although on average the models are biased cold in the Atlantic Water (MMM of -0.44°C), they are warmer than the climatology at 2000 m depth (MMM of 1.14°C) and at the bottom of the Nansen basin (1.25°C). The salinity profile is also inaccurate: when in observations the AW is the salinity maximum, in 10/14 models the salinity continues to increase with depth. Consequently, the T-S diagram in the Nansen basin (Fig. 2c) is unrealistic for the majority of the models. Most models have a shape somewhat resembling that of the observations (black), but with peaks at the wrong temperature and/or salinity and of a largely inaccurate magnitude (see e.g. CanESM5, plain blue line). The least inaccurate is GFDL-CM4 (plain green line), despite an AW core lying on average 400 m too deep and the whole AW layer extending to 2000 m depth. One of the most inaccurate is NorESM2-LM, which has "geometric" hydrographic profiles. This

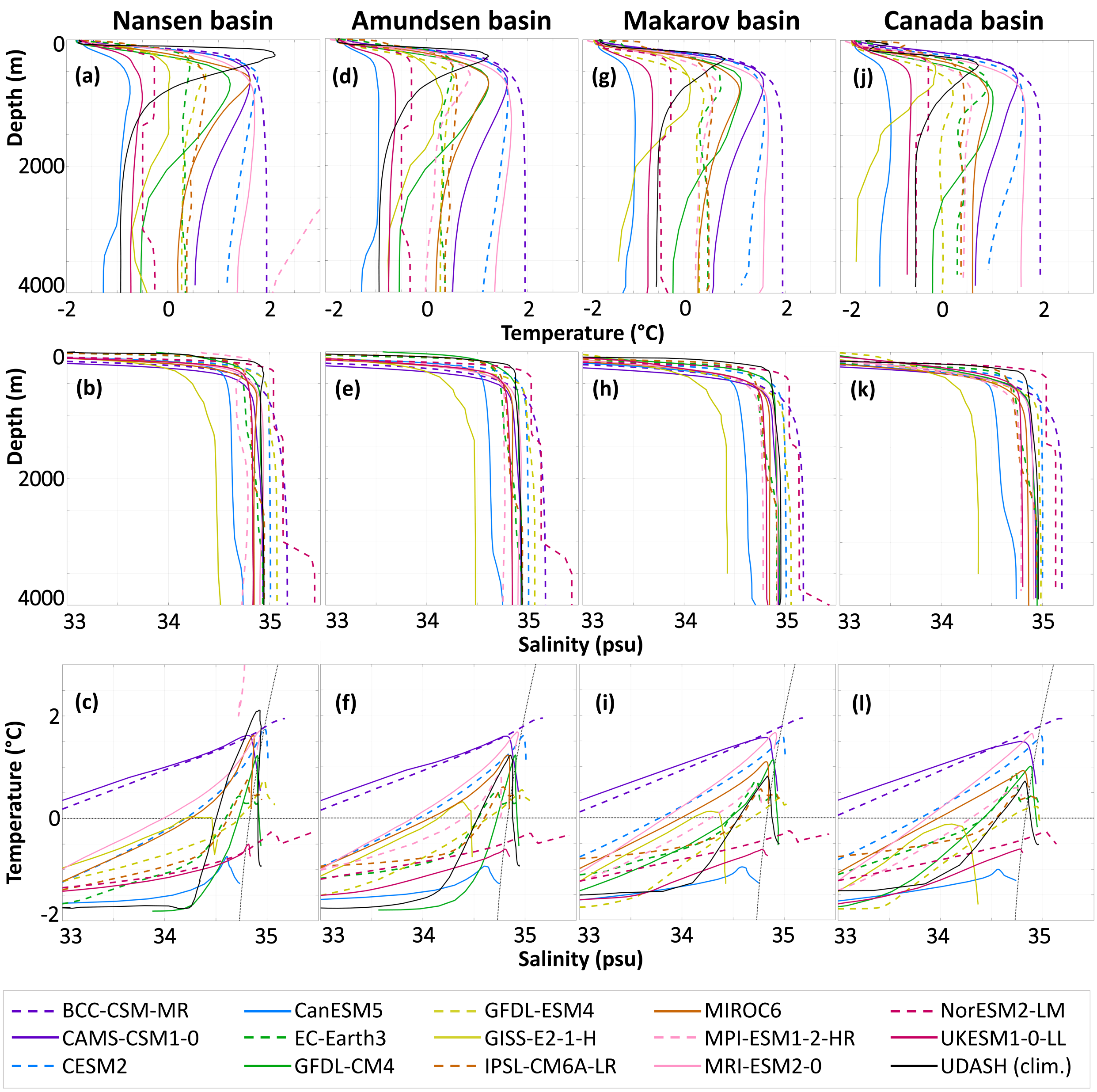

FIG. 2. Area-weighted mean temperature (top) and salinity (middle) profiles with depth, and corresponding T-S diagram (bottom), for each CMIP6 model and the observations in UDASH (Behrendt et al. 2018), for each of the deep Arctic basins. MPI-ESM1-2-HR is not visible on panel a) as its temperature is biased too warm (over 10°C in the upper ocean). On the T-S diagrams, the black dotted lines indicate the 0°C isotherm and 27.97 kg m^{-3} isopycnal.

is because on its native isopycnic grid (not shown), as the model is comparatively unstratified, some density classes occupy hundreds of metres. On average, the models are less stratified than observations: they have a dense bias in the AW and a light bias in the deeper layers; this result will be important in subsection 3b when investigating the ventilation.

All four deep basins exhibit the same biases: the Atlantic layer is too deep, too thick, and in some cases occupies the entire depth of the basin (Fig. 2). This suggests that the biases throughout the water column are linked, which they are (Fig. 3). For all basins, the across-model relationship between any two properties of the different water masses in that basin is split in two distinct depth levels:

- The biases in the upper 100 m are strongly correlated to each other: warm biases are associated with salty biases, which are associated with dense biases, which are associated with a weak stratification. These suggest that the wrong water mass is at the surface, but investigating this is beyond the scope of this paper. What is relevant for this study is that the biases in the upper 100 m are not correlated to those of the other water masses (empty squares in the top four lines, Fig. 3).
- From the Atlantic layer down, the biases in all properties and water masses are positively correlated to each other. As our definitions artificially split the Canada Basin Deep Water in two different water masses (2000 m depth and bottom), we expect a strong correlation between these two depth levels in the Makarov and Canada basins. However, the correlations are larger than 0.9 across all basins and depth levels (diagonal of deep red values, Fig. 3), and the actual values nearly align along the unit line when plotted against each other (not shown). As suspected from Fig. 2, most models in our study do not have distinct deep water masses, but rather fill the deep basins with a similar water from the Atlantic Water level to the seafloor.

Note that Fig. 3 was created using the area-weighted means, but the same results were found if using the area-weighted RMSE or the actual properties. Finally, the reader may have noticed that the Atlantic Water core depth (AWCD) is not correlated to any other property – we will come back to this finding later in the manuscript.

In observations, the properties of each water mass evolve not only with depth but also horizontally. Most visibly, the Atlantic Water becomes colder, fresher, deeper and thicker, and consequently results in a less pronounced peak on the T-S diagram as it travels from the Nansen basin to the Canada basin (black lines, Fig. 2). We do not observe this in models. AW density and temperature show little change across the Arctic. As a result, the biases (supp. Tables A1 to A3) change primarily because the value in the reference climatology changes rather than the values in the models. This is most visible when the properties are mapped (Fig. 4 and supp. Figs. A1 and A2): the AW appears biased dense and cold the most in the Nansen basin, as it is the basin where the density is lowest and temperature highest in the climatology. The maps reveal that no basin is better represented than the others; rather, the difference is largest when comparing the different water masses (RMSE, value on Fig. 4), and when comparing the deep basins to the shelves. No model clearly outperforms the others, and instead the model with the lowest bias depends on the depth and property considered (Fig. 4 and supp. Figs. A1 and A2, second row).

As for the evolution with depth, we verify that for each water mass its biases are consistent throughout the Arctic as suggested by Fig. 4 by computing the across model correlations between the basins (Fig. 5). For the four deep basins, the temperature and the salinity, and the three water masses, the correlations often exceed 0.9 (dark red on Fig. 5). There are two exceptions:

- On the Siberian shelf, there are no correlations with the deep basins. This suggests that the majority of models do not accurately represent the connection between the Siberian shelf and the deep basin via dense water overflows. We investigate this further in the next subsection.
- On the Greenland shelf, there are no significant correlations in salinity but strong correlations in temperature, especially with the AW in the deep basins. This suggests that the flow of Atlantic Water from the deep basins southward through Fram Strait may be accurately represented. We investigate this further in the next two subsections.

In summary, across CMIP6 models the Atlantic layer is biased cold, fresh, and dense when compared to observations, while the deep and bottom waters are biased warm, fresh, and light. The biases between water masses are strongly correlated to each other, and coupled with the fact that the AW occupies nearly the entire water column in most models, suggest that the different water masses are not significantly different from each other. The biases are also consistent throughout the Arctic. In the next subsection, we investigate whether this lack of variation with depth and with distance is caused by inaccurate ventilation and circulation of these waters within the Arctic.

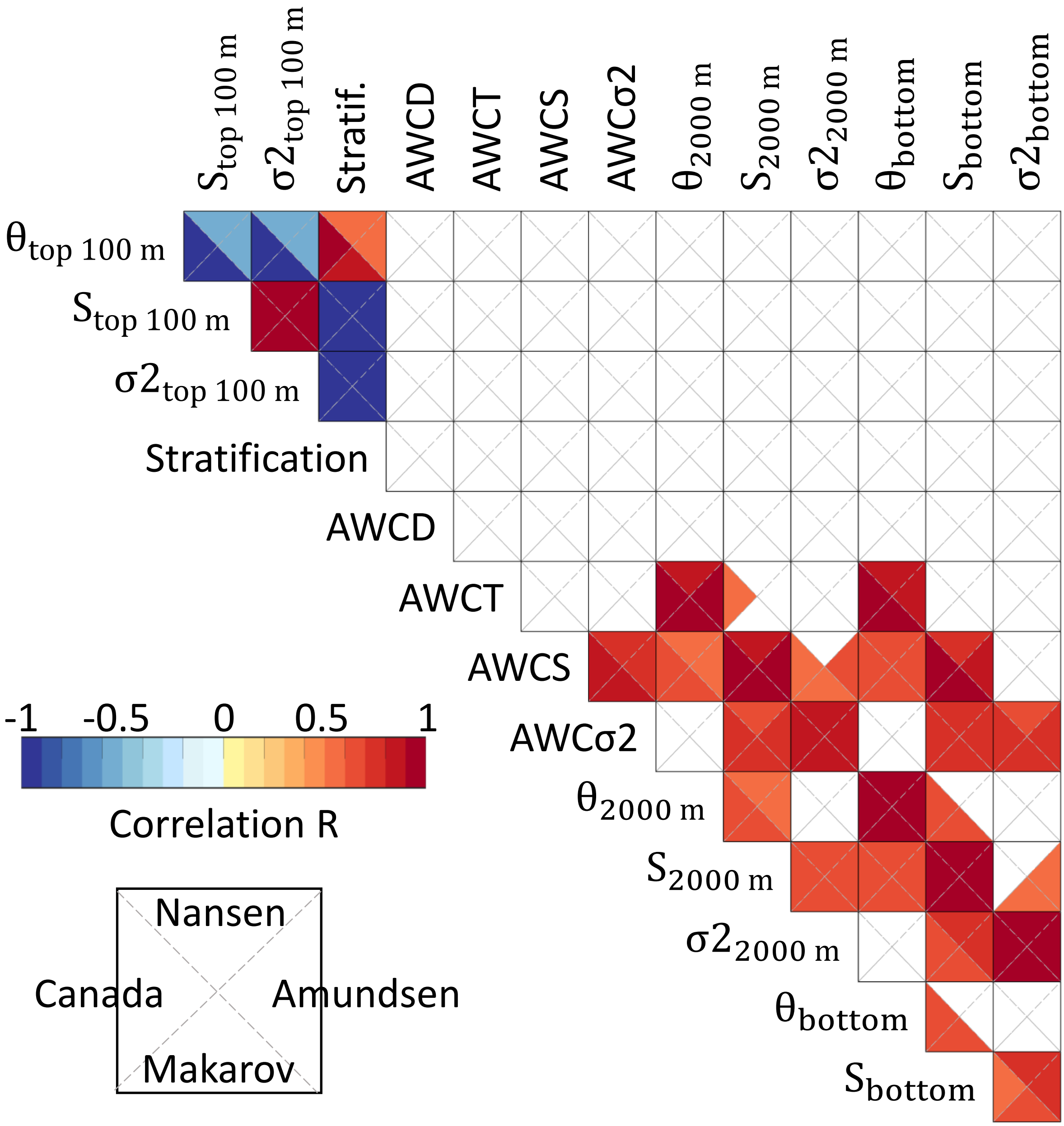

FIG. 3. Across-model correlation between the biases in water mass properties throughout the water column, for each deep basin (individual triangles): Mean temperature, salinity and density of the upper 100 m as proxies for the halocline; stratification, i.e. density difference between the halocline and the Atlantic Water core; Atlantic Water core depth (AWCD), temperature (AWCT), salinity (AWCS) and density (AWCσ2); temperature, salinity and density at 2000 m depth as proxies for the deep water; and temperature, salinity and density at the bottom. See methods for more information. Only correlations significant at 95% level shown (non-significant correlations are white).

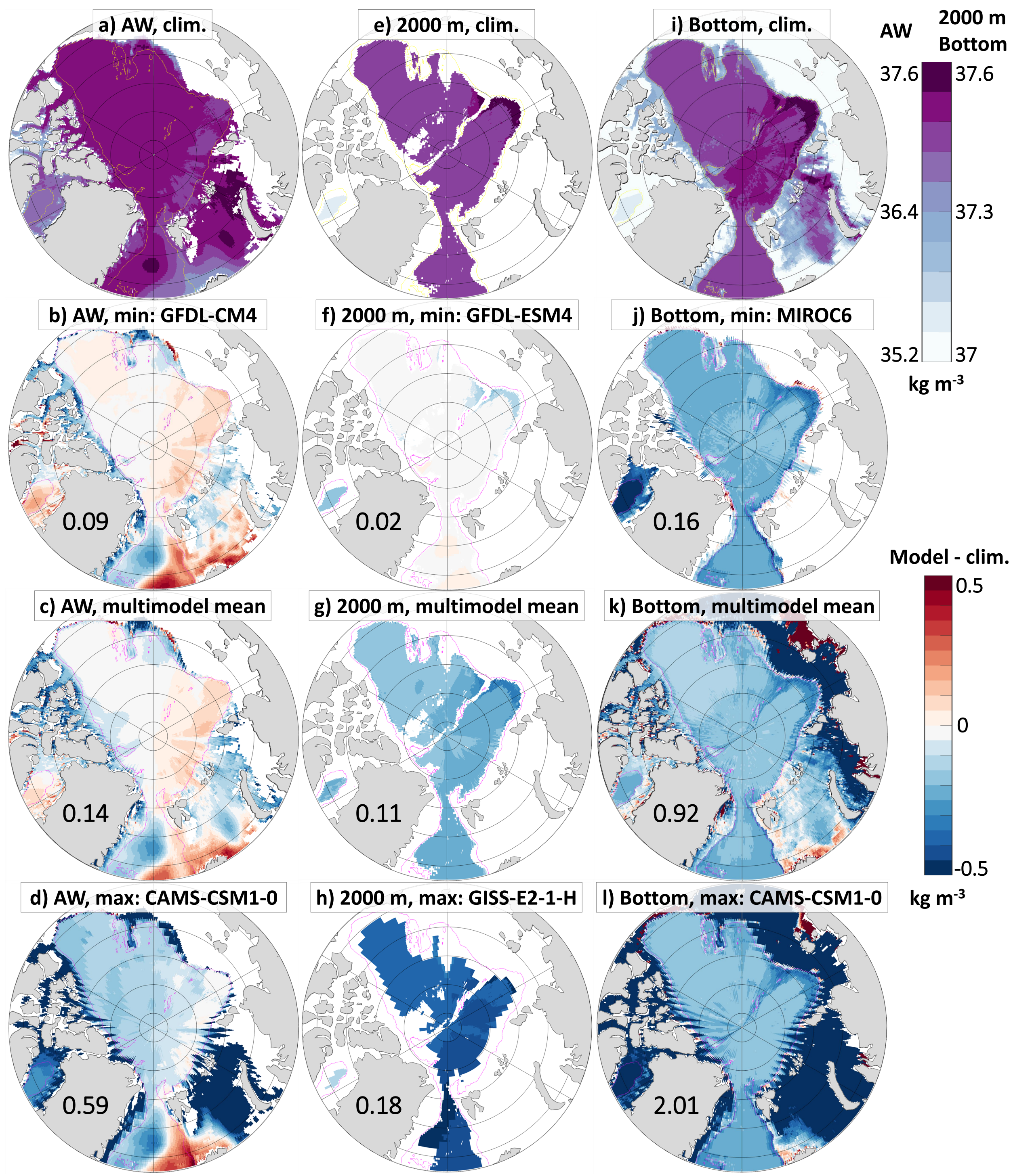

FIG. 4. Density σ_2 in the WOA18 climatology (top row) and bias when compared to this climatology for the least biased model (second row), the multimodel mean (third row) and the most biased model (last row), for the Atlantic Water core (first column), 2000 m depth (second column), and the bottom (last column). The numbers are the respective Pan-Arctic area-weighted root mean square errors. See supp. Figs A1 and A2 for the temperature and salinity.

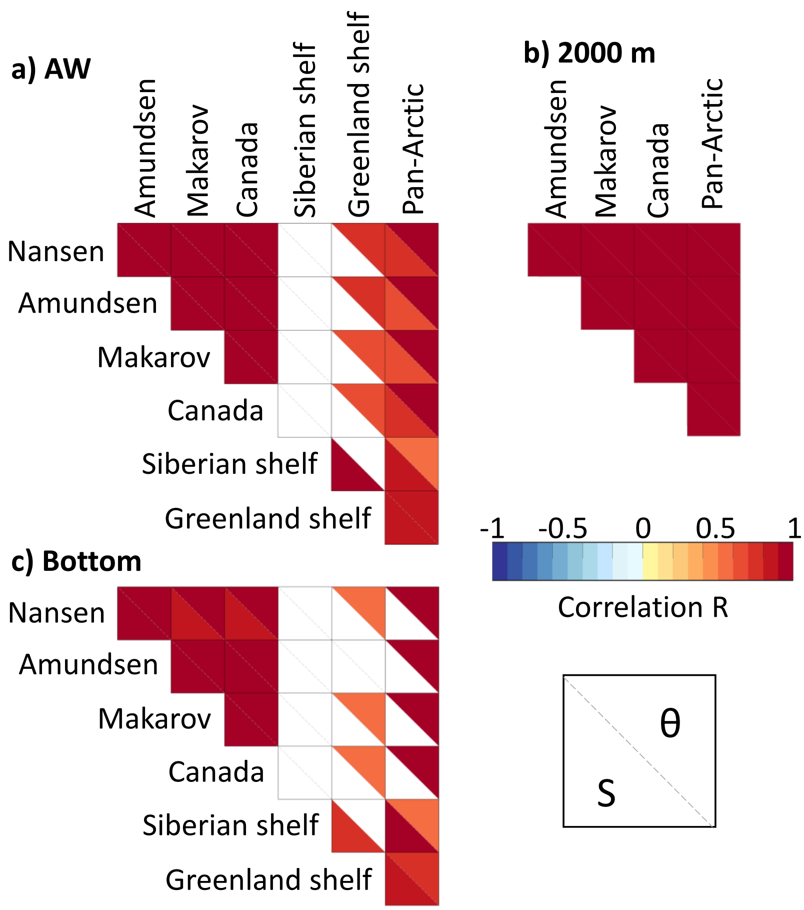

323 FIG. 5. Across-model correlation in the biases in each water mass temperature θ and salinity S between regions,
324 for a) the Atlantic Water core, b) the deep water at 2000 m depth (no value on the shelves as per shelf definition),
325 and c) the bottom. See methods for more information, in particular for the regions' definitions. Only correlations
326 significant at 95% level shown.

b. Ventilation and circulation of deep water masses within the Arctic

We just showed that there is no across-model correlation between the Atlantic Water and deeper ocean biases and those in the upper ocean. This means that the deep biases may come from an inaccurate representation of the processes that normally form or modify those deep waters. We start with the processes that take place within the Arctic, and in particular with dense water overflows.

Of the 8/14 models that provided the age of water as a parameter, only two appear to simulate overflows at the Arctic shelf break (Fig. 6a and d, regions highlighted with green boxes): NorESM2-LM, through Franz-Victoria Trough and St Anna Trough; and MIROC6, through St Anna Trough only. For both these models, the overflow is visible as a continuous 0 to 1 year age on either side of the 1000 m isobath. We attempt to track these overflows as they travel off the shelf break, but both in animations (not shown) and in sections across (Fig. 6b and e) and along (c and f) the shelf break, we can only detect the occasional grid cell with a low age and not a clear flow. These suggest that NorESM2-LM may ventilate down to 3000 m depth occasionally, and MIROC6 to 2000 m. These two models also have the least biased deep and bottom waters for the entire Arctic (see previous section). One of the reasons for these models' relatively good performance may be their different vertical grids than the other 6 models in this subsample (isopycnic and terrain-following, respectively), which should be particularly well-suited to represent a density-driven flow along a slope.

For the remaining 6/14 models, we use bottom density as a proxy for ventilation. Only GFDL-ESM4 may have a dense water overflow, in St Anna Trough (Fig. 6g), but tracking its progression down the shelf (Fig. 6h,i) is not trivial. Referencing the density to different depth levels did not make the result clearer. As GFDL-ESM4 is the model that we previously found to have the least biased 2000 m salinity and density, it is possible that it has overflows. Besides, GFDL-ESM4 and NorESM2-LM are able to simulate overflows on the Antarctic shelf break (Heuzé 2021), which suggests the potential for them to do the same in the Arctic. Either way, previous studies have shown that overflows occur at several other locations, including at the Canadian shelf break (Luneva et al. 2020). Of the 14 models we study here, however, only 3 models show indications of simulating overflows, all in the same troughs. This leads us to a natural follow up question: How do the other models ventilate their deep waters, if at all?

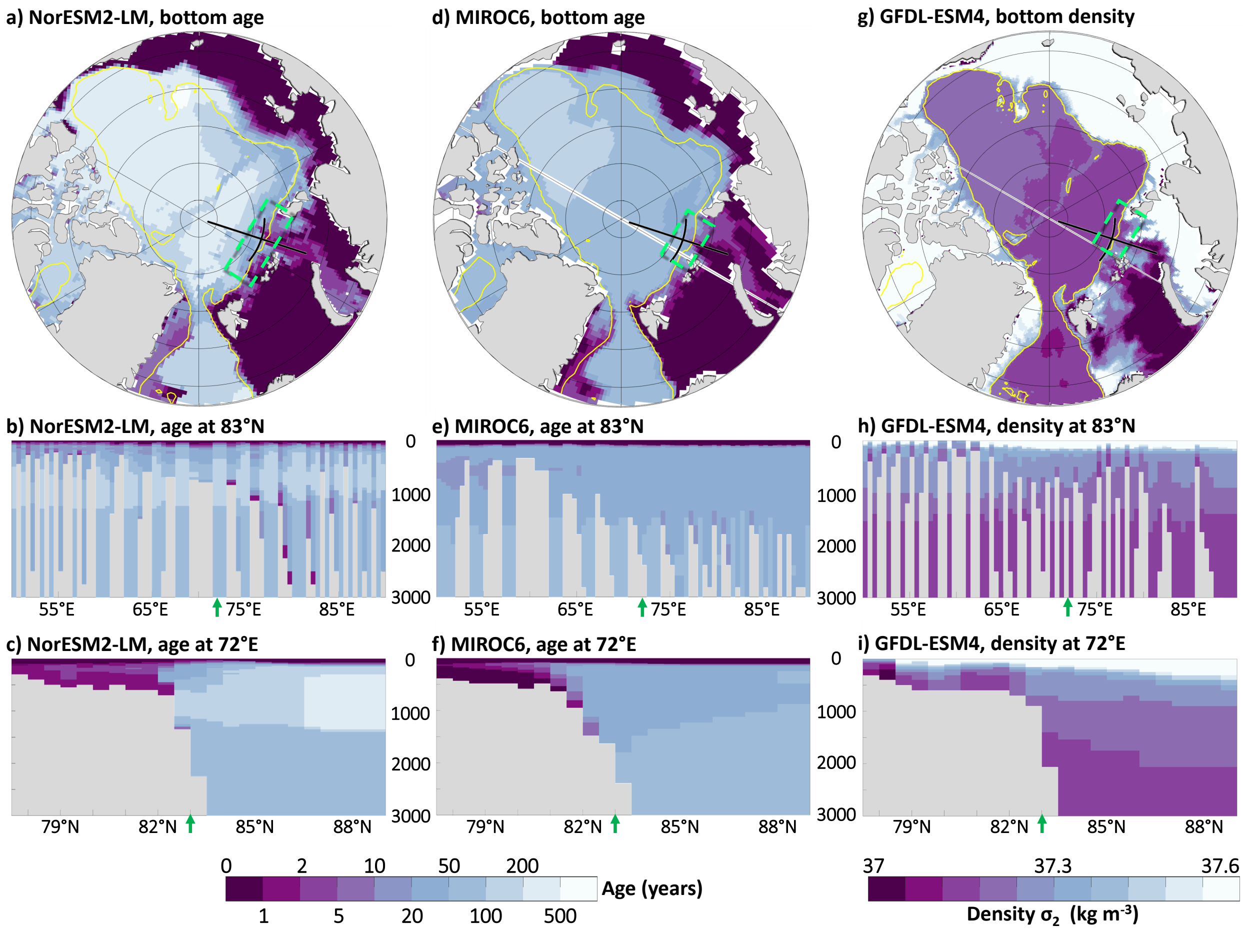

FIG. 6. For the three models that appear to have overflows, top: For the whole Arctic, map of the minimum age of water / maximum density σ_2 at the deepest grid cell (shading) and 1000 m isobath (yellow line), where a low age / high density on either side of this isobath suggests overflowing at the shelf break. Green boxes highlight the location of such overflow; black lines, the location of the sections on the other panels. Centre and bottom: Sections along (83°N) and across (72°E) St Anna Trough of the age of water / density σ_2. Note the logarithmic colour scale for the age.

The Arctic Ocean is too stratified for open ocean deep convection to occur (Rudels and Quadfasel 1991). However, using the high resolution climate model HiGEM and a four times increase in CO_2 scenario, Lique and Thomas (2018) found that open ocean deep convection can start in the central Arctic. Considering that the models in this study are less stratified than observations (subsection 3a), we verify whether they ventilate the deep Arctic via open ocean deep convection. The only model with deep mixed layers in this study is GFDL-CM4, which reaches a maximum of 1815 m in the Nansen basin (supp Fig. A3 - note the logarithmic colour scale). The second deepest is EC-Earth3, with a maximum of 536 m. All the other models have mixed layers shallower than 100 m on average over the deep Arctic basins, never exceeding 250 m. Considering that we found a deep bias in the Atlantic layer, this means that GFDL-CM4 and EC-Earth3 are the only two models whose mixed layers can reach below the halocline. As previously discussed, GFDL-CM4's Atlantic layer extends deeper than 2000 m, so its comparatively deep mixed layer still cannot ventilate the deep and bottom waters.

In summary, we found three models that show indications of dense water overflows in St. Anna Trough that may penetrate below the Atlantic Water, and two models that ventilate the Atlantic layer via open ocean deep convection. Our last hypothesis was that deep and bottom waters may not be ventilated at all, and simply relaxing from the climatology they were initialised with (listed in Table 1). We tested this hypothesis by computing the biases in water mass properties when compared to each model's climatology rather than WOA18: if the biases had been reduced, the hypothesis could have been correct. Unfortunately, the changes in the biases are not consistent across models or across parameters (not shown), and only reflect the differences between the climatologies. This result was to be expected, as changing even the deepest waters is the reason why models are spun up for hundreds to thousands of years (e.g. Stouffer et al. 2004; Bernsen et al. 2008, and references listed in Table 1).

We leave for now the partially-unresolved question of the ventilation and instead investigate the representation of exchanges across the Arctic below the surface, first for the subset of models that provided the age of water output. Tanhua et al. (2009) estimated the age of water in the Arctic Ocean from transient tracer measurements (Fig. 7a). The age of water in the models looks drastically different. In the upper ocean (top panels of Fig. 7), the models can be split in two groups:

- Most models seem to "spill over", i.e. below 200 m depth, the age gradually increases from the shallow levels of the Nansen basin by the Kara Sea (to the right) towards the deep parts of the Canada basin by Alaska (to the left). These models are IPSL-CM6A-LR (Fig. 7d), MIROC6 (e), MPI-ESM1-2-HR (f), MRI-ESM2-0 (g), UKESM1-0-LL (i), and to some extent CESM2 (b).

- The other two models CanESM5 (c) and NorESM2-LM (h), and to some extent again CESM2 (b), have waters that are much older than the observations between 200 and 1000 m depth throughout most of the deep Arctic (up to 500 years older for CanESM5), albeit with a mild doming of young waters deeper over the Mendeleev Ridge - opposite to the observations.

In the deeper levels, most models are either uniformly younger (MIROC6, MPI-ESM1-2-HR, MRI-ESM2-0, and UKESM1-0-LL) or older than the observations (CESM2, CanESM5, IPSL-CM6A-LR). The oldest waters in MRI-ESM2-0, the model with the largest young-bias, are 122 years old; in CanESM5, the model with the largest old-bias, 1946 years old. One important caveat is that the OMIP protocol recommended the model age be reset to 0 at the beginning of the historical run (Griffies et al. 2016). This recommendation was followed in the four "young" models (MIROC6, MPI-ESM1-2-HR, MRI-ESM2-0, and UKESM1-0-LL), while in the four "old" models (CESM2, CanESM5, IPSL-CM6A-LR, NorESM2-LM) instead the age was set to 0 before the spin-up began and not reset since (personal communication with the modellers listed in the acknowledgments, March 2022). Note that for the study we conduct here, the latter method is most desirable. Three out of the four models whose age was reset in 1850 have an oldest age lower than 165 years old, i.e. lower than the duration of the historical run (MIROC6, 139 years; MRI-ESM2-0, 122 years; UKESM1-0-LL, 129 years), suggesting that these models have true fast processes and that this is not simply an effect of the reset.

The models at least all reproduce the contrast between the Eurasian basin (Fig. 7, right) and the Canada basin (left): in the deep Eurasian basins, waters are younger to a deeper level than in the Canada basin. The one model that sticks out for its relative accuracy is NorESM2-LM (Fig. 7h), with young AW overlaying older water in the Amundsen basin, 200 year old waters in the Makarov basin, and the oldest waters in the Canadian basin, potentially again a result of its vertical grid that allows the isopycnals to wrap over the Lomonosov Ridge. What these ages suggest is that the circulation in the upper levels is inaccurate: instead of looping in the Eurasian basin (visible in the observations as a band of young waters from the surface to 1000 m), the models seem to flow across that basin and into the Canada basin. This was also shown by Muilwijk et al. (2019), who used passive tracers in a coordinated study of 9 ocean models and found large discrepancies in the Atlantic Water flow pattern in the Arctic Ocean. The circulation in the deeper levels also appears to be inaccurate, not so much in its route, but rather in its speed. The strong significant correlation between the age of the Atlantic Water on the Greenland shelf and the age of that water (-0.71, i.e. older water is colder) also suggests that the circulation may be inaccurate. That is, in the models with the older and colder water, the flow may be slower than in the models with younger and warmer waters, or the flow may be taking different routes. We therefore now investigate the velocity fields of the models.

We compare one of the “young” models, MIROC6, and the “oldest”, CanESM5, in Fig. 8. These two models were chosen because their horizontal grids are not significantly rotated compared to the Cartesian reference, therefore the velocity components ‘uo’ and ‘vo’ are meaningful on the models’ grids. The value of the velocity is shown for all other models on supp. Figs. A4 and A5. As expected, these two models differ significantly both in the magnitude of their ocean velocity and in its direction. In MIROC6 (Fig. 8a), the Atlantic Water flows in an orderly loop around the Eurasian basin at 2 cm/s or faster, i.e. the same order of magnitude as measured by the Eastern Eurasian Basin moorings of Woodgate et al. (2001) and Pnyushkov et al. (2015). The flow in CanESM5 (Fig. 8b) is four times slower and less orderly, with a lot of recirculation within the Eurasian basin. The AW also recirculates more in the Makarov basin in CanESM5 than in MIROC6, but in the Canada basin, they look somewhat similar, although again MIROC6 is twice as fast. At 2000 m, the circulation in the Eurasian basin is very similar to that of the AW for both models (Fig. 8c and d), probably because as discussed previously, the same water mass is found at the depth of the AW core as at 2000 m in most models. In MIROC6 it is no issue for the water to flow from the Makarov basin towards the Canadian shelf, but in CanESM5 the water loops around a shallow feature, most likely the model’s interpretation of the Alpha Ridge. Aside from that loop, MIROC6 shows again velocities twice as high as CanESM5. The absolute velocity does not seem to be the key element for ventilation though; for example, CESM2 and UKESM1-0-LL (supp. Fig. A4c and l) have similar velocities in each basin, yet very different ages, even taking UKESM1-0-LL’s age reset into account. IPSL-CM6A-LR and NorESM2-LM in contrast have similar ages but very different velocities both in the Atlantic layer and at 2000 m depth (supp. Figs A4 and A5, h and k), with NorESM2-LM being up to 100 times as fast as IPSL-CM6A-LR locally. In summary, the age difference on Fig. 7 likely is the result of a more organised flow rather than flow speed only, both in the Atlantic layer and deeper.

What causes these differences in circulation? We find significant, negative across-model correlations between the depth of the Atlantic Water core and its velocity in each basin (-0.47 in the Nansen basin; -0.62 Amundsen; -0.46 Makarov; -0.42 Canada). That is, the slower the core,

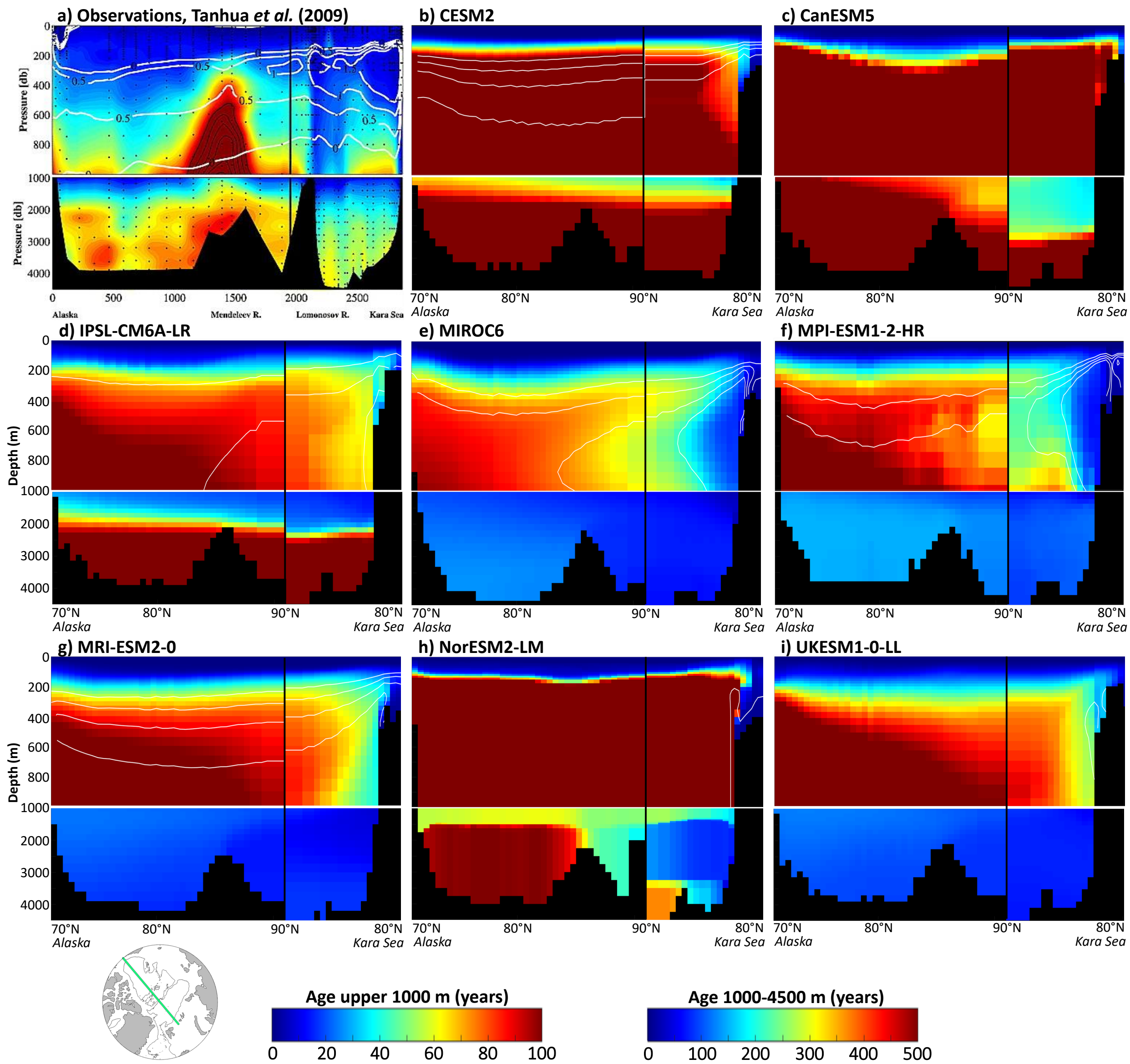

FIG. 7. Age of water across the deep Arctic basins a) as reported by Tanhua et al. (2009) (reproduced with permission from John Wiley and Sons, license number 5239230975302) and b)-i) for the 8 CMIP6 models of our study that provided this output. See Tanhua et al. (2009) for exact locations of their measurements; in CMIP6 models, section goes along 140°W to the North Pole, then along 40°E (green line on the map, bottom left corner). Black vertical line marks the Canadian-Eurasian basins separation. White lines on top panels, the 0, 0.5, 1, and 1.5°C isotherms.

the deeper. It is unclear however what the causality is, i.e. whether the flow is slower because it is deeper or deeper because it is slower. Another thing we notice is the impact of horizontal

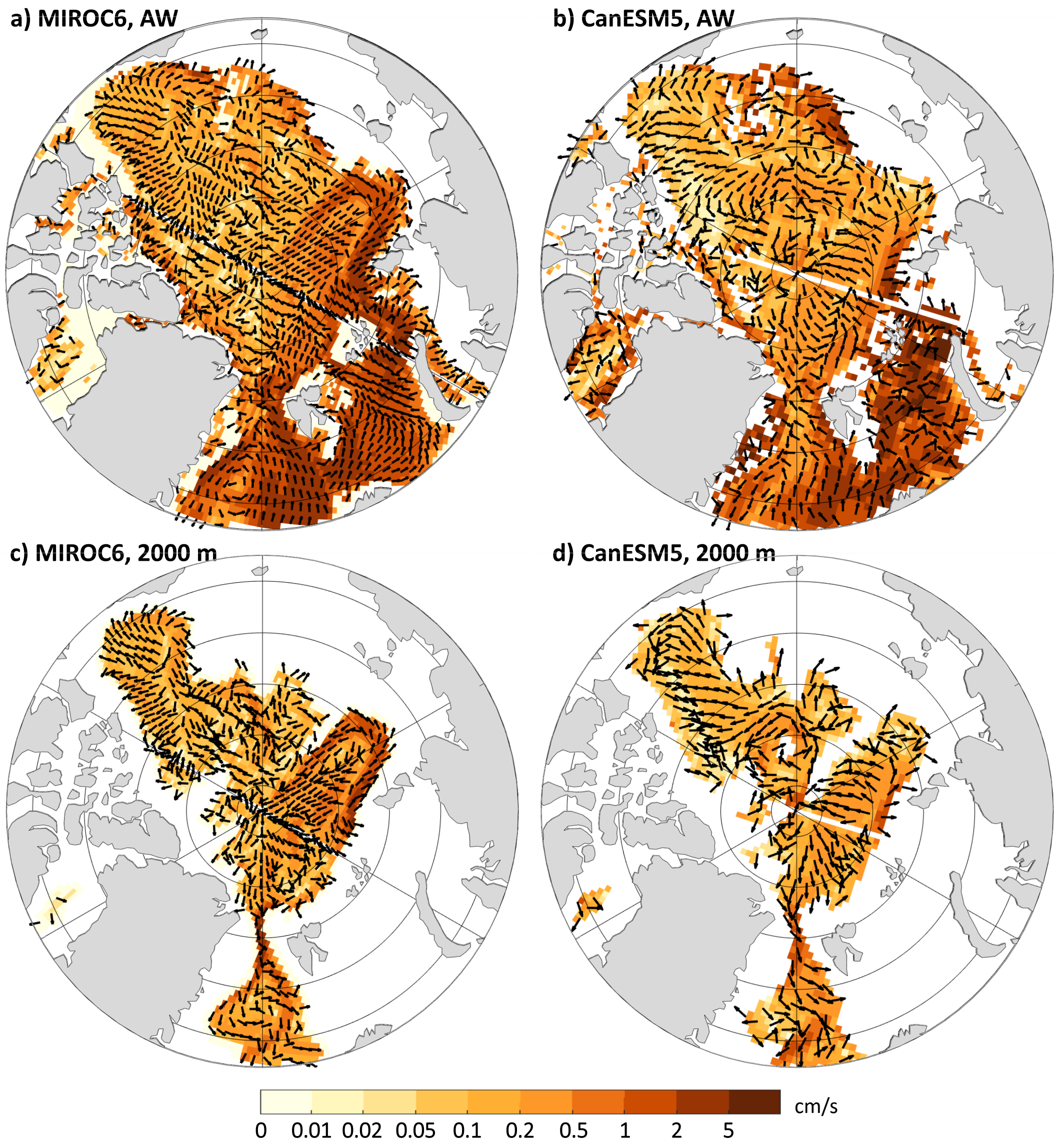

FIG. 8. Velocity (shading) and direction of the flow (arrows) for one of the models with the youngest waters, MIROC6 (left), and the one with the oldest, CanESM5 (right), at the Atlantic Water core (top) and 2000 m depth (bottom). Note the logarithmic scale for the velocity. For increased readability, the velocity vectors have been normalised, so all arrows are of the same length. The velocity norm is provided for all the other models in supp. Figs A4 and A5.

resolution, notably when comparing the very high resolution GFDL-CM4 (9 km) to the others (40-50 km): at this resolution, the meanders and recirculations can be clearly represented (supp. Fig. A4e). The effect of resolution on Arctic circulation was also investigated by previous studies:

for example, Docquier et al. (2019) and Docquier et al. (2020) show that higher ocean resolution intensifies the Atlantic Water currents and allows to better resolve the different oceanic pathways into the Arctic. Docquier et al. (2020) further note that eddy-permitting ocean resolution results in improved circulation in comparison to observations, as we see with GFDL-CM4. Roberts et al. (2016) also found that a higher ocean resolution leads to stronger boundary currents. Furthermore, differences in model diffusivity may result in different flow speeds – some models might be more diffuse than others, meaning they can have similar overall volume transports but large biases in velocity as the currents are less confined to the coastal boundaries due to excessive mixing (as was found for the North Atlantic by Talandier et al. 2014). Atmospheric biases is another likely explanation for differences in Atlantic Water flow speeds and patterns, as recently demonstrated by Hinrichs et al. (2021) whose realistic Atlantic Water circulation worsened after coupling to a biased atmospheric model. Finally, Karcher et al. (2007) showed that for early versions of Arctic Ocean models, the balance of potential vorticity is also important and closely linked to the intensity and the pattern of Atlantic Water flow. Steep topographic features such as the Lomonosov Ridge can create a potential vorticity barrier, thus differences in the momentum advection schemes and momentum closure schemes might also lead to differences among the models.

While we can speculate on the reasons for these different flow speeds and paths, their study would require that

- The ocean velocities be archived for all models;
- The necessary information to reproject the velocities onto the Cartesian grid be included in the output files, e.g. via an angle parameter that for each grid cell gives its rotation compared to the true north;
- The age of water be archived for all models;
- The age has the same definition for all models. In particular, resetting the age to 0 at the beginning of the historical run seriously impacts any study of the deep ocean.

In summary, in this subsection we have shown that a minority of models ventilate their Atlantic Water, and one potentially its deep waters, via exchanges with the surface within the Arctic. Half of the models, however, have deep and bottom waters that are biased young. This is linked to a more structured flow that efficiently transports the water from the Nansen to the Canada basins, suggesting that what enters the Arctic through Fram Strait controls the properties in the whole deep Arctic. In the following subsection, we therefore investigate these flows through Fram Strait.

c. Exchanges through Fram Strait

The representation of Fram Strait in our selection of CMIP6 models itself is quite biased, be it in properties or in fluxes. When compared to WOA18 (Fig. 9), most models are biased cold in the upper ocean where WOA18 is warm, and biased warm in the deeper layer where WOA18 is cold. In other words, their temperature contrast between the upper and deeper ocean is too small. We observe the same pattern in salinity to some extent (supp. Fig. A6), with strong saline biases in the upper ocean towards Greenland (left of the panels) where WOA18 is freshest, but in the rest of the strait there is no across-model consistent bias. The biases in Fram Strait have a strong and significant across-model correlation to the property biases in the Nansen basin described previously: 0.84 between the Fram Strait inflow and the Nansen basin Atlantic Water core for the salinity and 0.74 for the temperature, reduced to 0.78 and 0.56 respectively when comparing the Fram Strait inflow to the Nansen basin bottom properties. The Nansen basin biases are also strongly correlated to the bottom property biases in the Nordic seas from Heuzé (2021), the largest correlation being 0.81 (0.83) between the Nordic Seas bottom salinity (temperature) and that in the Nansen basin at 2000 m depth, suggesting that the biases are advected from the south (upstream of Fram Strait) and into the Arctic. We verify this hypothesis below.

The location of the inflows and outflows is also inconsistent across models (black contours, Fig. 9). Using the moorings deployed across Fram Strait, Beszczynska-Möller et al. (2012) showed the presence of a strong outflow, i.e. flow out of the Arctic, to the west, a strong inflow to the east, and several recirculations in the centre of the strait. Although in- and outflows are in fact flows of different water masses (von Appen et al. 2015), the patterns are nonetheless quite consistent through depth. The models show instead a large range of behaviours, for example:

- BCC-CSM2-MR and CAMS-CSM1-0 do not simulate a separation by longitude but by depth, where the upper ocean is an outflow, intermediate depths (the majority of the water column) is an inflow, and anything below 2000 m is again an outflow;
- CanESM5, EC-Earth3, IPSL-CM6-A-LR, MPI-ESM1-2-HR and UKESM1-0-LL simulate an inflow that is limited to a strong core along the east coast, extending no deeper than 1000 m;

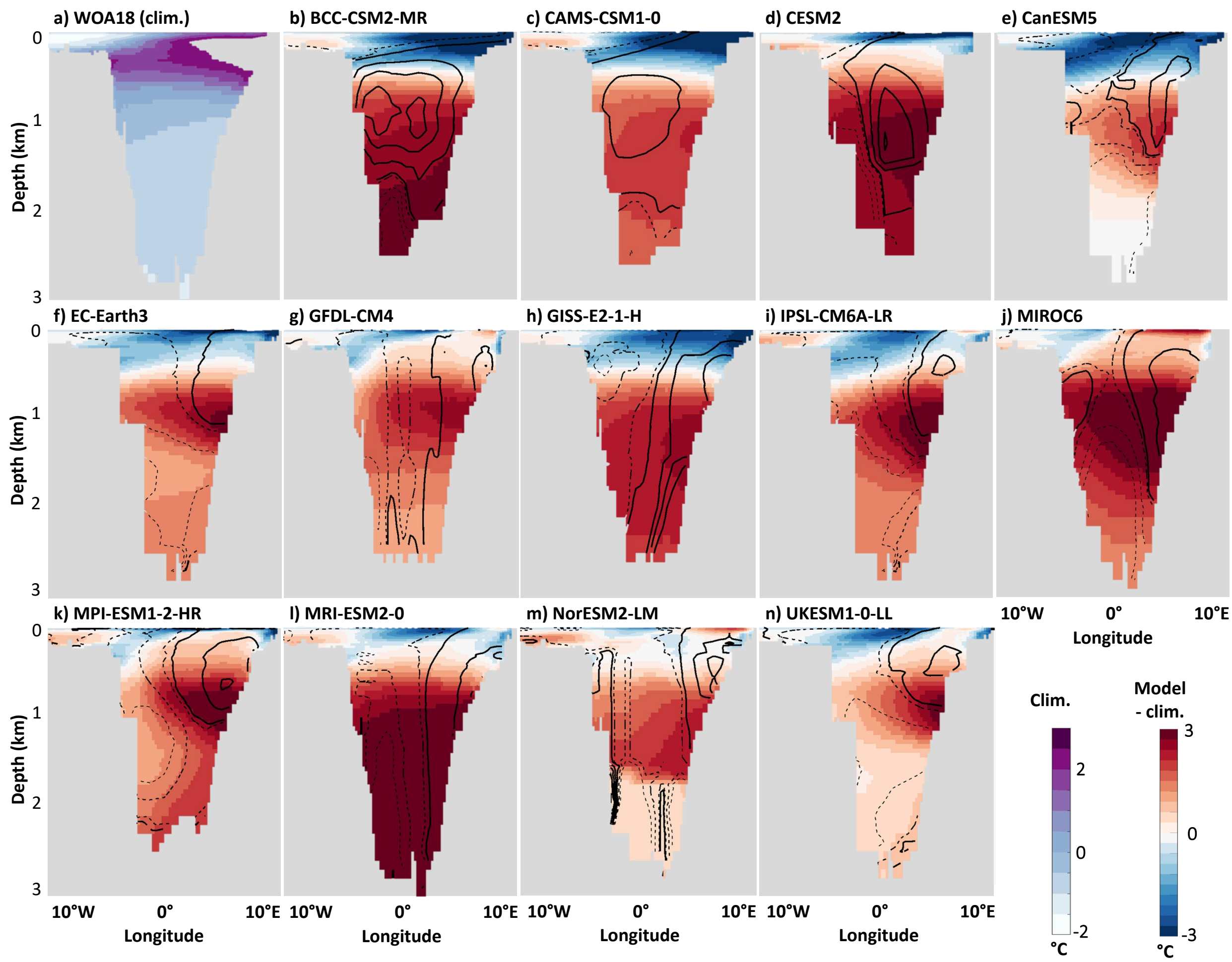

FIG. 9. a) Potential temperature across Fram Strait in WOA18; b)-n) difference between each model's potential temperature and that of WOA18 across Fram Strait (shading), along with their volume flux as black lines (0.02 Sv contours, where 1 Sv = 10^6 m^3 s^{-1}; plain means positive, into the Arctic; dashed negative, out of the Arctic). Salinity biases are shown in supp. Fig. A6

- GFDL-CM4, GISS-E2-1-H and MRI-ESM2-0 simulate a binary circulation, with an outflow to the west and inflow to the east, which is correct. They however lack the observed recirculations (i.e. alternation of in- and outflows) to be deemed accurate.

Fram Strait is biased warm and the location of the in- and outflows is inaccurate in all models, at least when compared to the mooring data of Beszczynska-Möller et al. (2012). It is therefore not surprising that the heat and volume fluxes through Fram Strait are inaccurate as well. Note that as the salt fluxes strongly resemble the volume fluxes and uncertain observational values were only mentioned in Marnela et al. (2016), we limit our discussion to the heat and volume fluxes. Besides, in contrast to observational data, the models do not have distinct east/west and upper/deeper fluxes. We therefore discuss here the full-depth net fluxes into and out of the Arctic, i.e. the sum of the positive and negative fluxes, respectively. For the heat flux (Fig. 10a), most models are within the observational range, except for GFDL-CM4, MIROC6 and MRI-ESM2-0 who overestimate both the inflow and outflow. For example with a 30-year mean value of 62.5 TW, the inflow in MIROC6 is nearly twice as large as that computed by Schauer et al. (2004) over 1997/1998 (31.8 TW). All models correctly simulate that the inflow of heat is larger than the outflow (difference of height between the bars), but this difference ranges from 1.4 TW for EC-Earth3 to 37.0 TW for MIROC6. One caveat is that where observational values are computed relative to different reference temperatures, we here computed them all relative to 0°C in order to easily compare the models to each other. We argue that as all the models of this study are biased warm in Fram Strait (Fig. 9), and that the across-model correlation between heat flux and temperature bias is only 0.49, i.e. explains only 24% of the variance, choosing a common reference temperature is not the leading reason for the differences between models.

Unlike the heat flux, the volume flux is underestimated in the majority of our models (Fig. 10b). Only the inflow of GFDL-CM4 and GISS-E2-1-H are within the observational range (averaged from Beszczynska-Möller et al. 2012; Marnela et al. 2016; De Steur et al. 2014; Schauer et al. 2004), and no model reaches the outflow observational range (11 ± 2 Sv, same references). Although all models except GISS-E2-1-H correctly have larger outflow than inflow, this difference is nearly twice the observational average (ca. 2 Sv) in CanESM5, IPSL-CM6A-LR and MIROC6 (3.5, 4, and 3.5 Sv on average, respectively), and less than half in BCC-CSM2-MR, CAMS-CSM1-0 and CESM2 (<1 Sv). We wonder whether these inaccurate differences between inflow and outflow through Fram Strait are compensated by the flows through the other straits and/or the solid fluxes, and therefore compare our results to those of Zanowski et al. (2021) for the five models we have in common. These suggest that:

- the more total solid freshwater flux out of the Arctic, the smaller our heat and volume outflows;
- the more total liquid freshwater flux out of the Arctic, the stronger our volume inflow.

Although these results would be logical, they should be investigated in a larger group of models; doing this here is however beyond the scope of this paper.

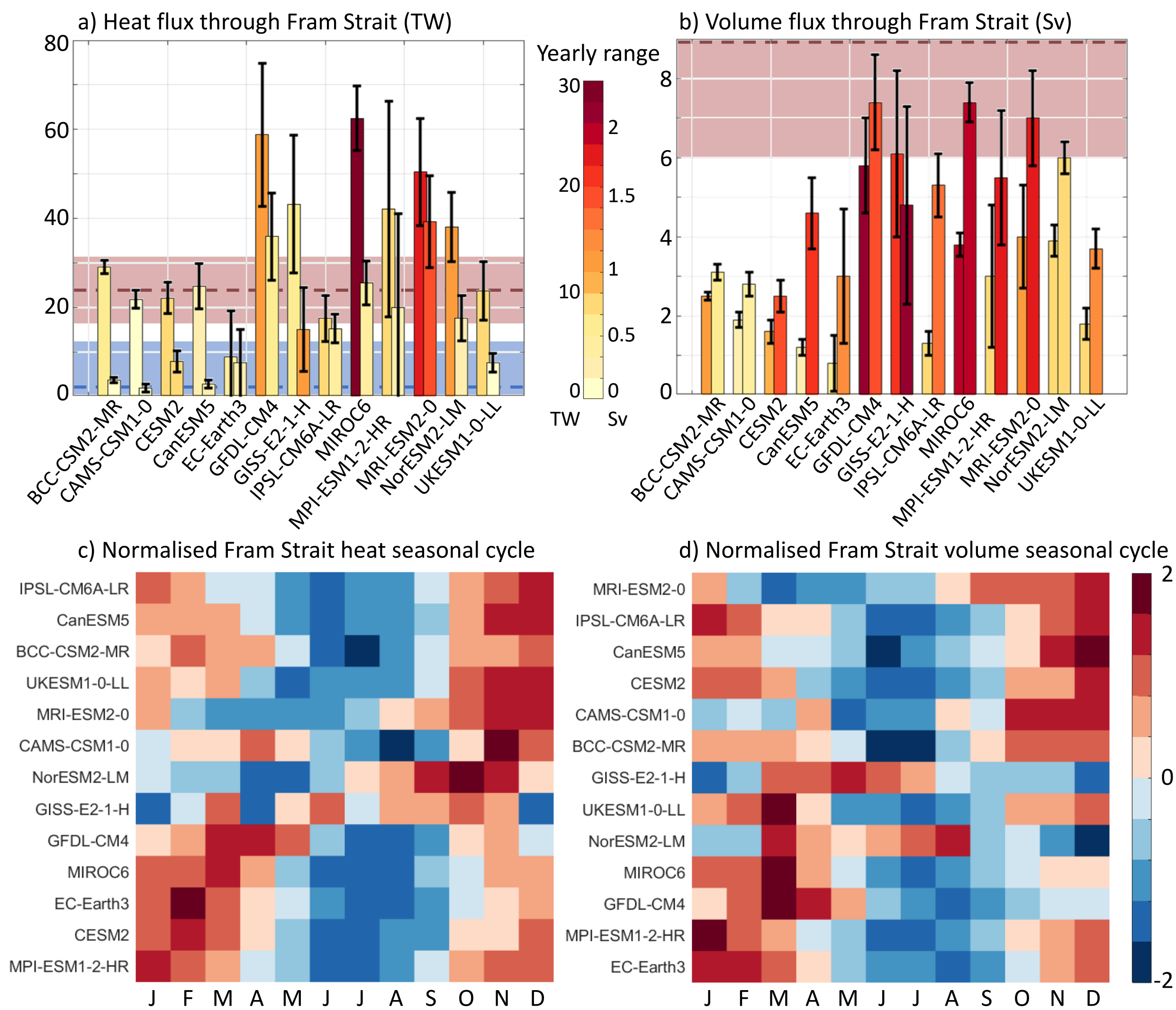

FIG. 10. For each model that provided the velocity outputs, a) Bars: 30-year mean heat flux, in TW, into the Arctic (left, backward) and out of the Arctic (right, forward); black error bars: interannual variability, i.e. spread in the yearly means; shading: difference between the yearly maximum and minimum; pink and blue boxes: range of the observational values (see text), with mean as dashed line, for the in- and out-flow, respectively. b) Same as a) but for the volume flux, in Sv (1 Sv = 10^6 m^3 s^{-1}); the observational outflow values are off-screen at 11 ± 2 Sv. c) and d), normalised seasonal cycle in heat and volume inflow, respectively, where the models are there ordered by month of their maximum value.

Could the biases in fluxes through Fram Strait explain the biases that we found in the deep water masses of the Arctic? At first glance, no: there is no across-model relationship between any of the biases described in subsection 3a and the net in- or outflows. We investigate the models individually

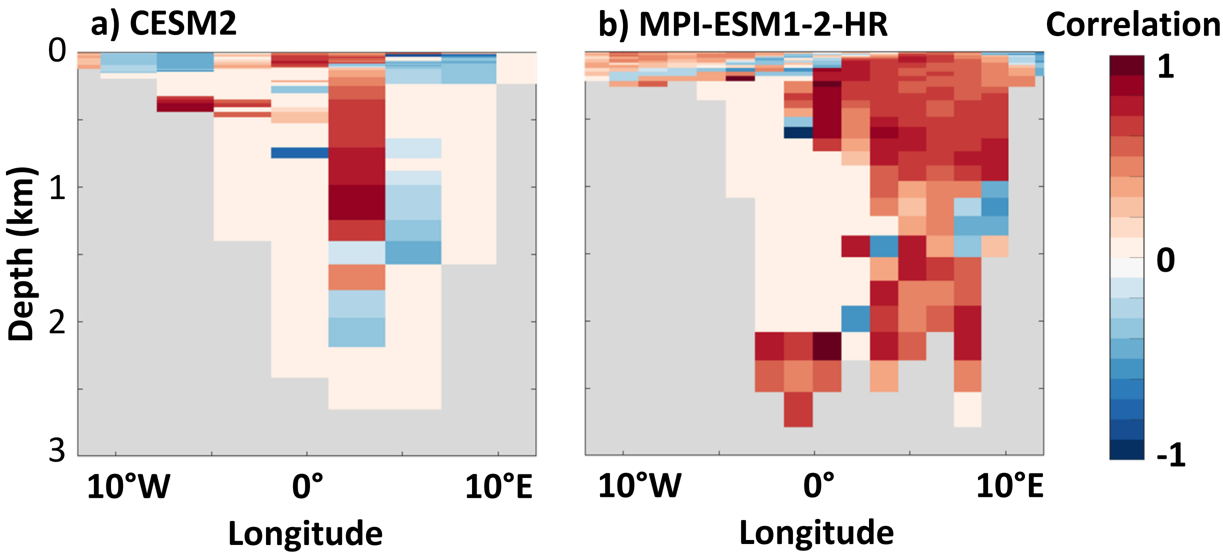

FIG. 11. For two exemplary models, correlation between the time series of yearly means in Atlantic Water core temperature in the Nansen basin and the heat flux into Fram Strait of each grid cell, allowing for a lag of up to 5 years. Only significant (at 95%) correlations shown. Note that this calculation was performed on the model's native grid, hence the difference in bathymetry from Fig. 9.

and compare their fluxes to the biases in Atlantic Water core temperature, in the Nansen basin only, as we previously showed that all property biases in all water masses and all deep basins were strongly correlated with each other. We find for all models, strong positive correlations between the fluxes and time series of the biases (see two exemplary models on Fig. 11), but no across model consistency. First, some have their strongest correlation with the heat flux, while others with the volume flux. But more importantly, for all models the whole inflow is not consistently correlated to the biases: some have a jet-like correlation, where a specific longitude has most of the positive correlation (Fig. 11a); others have distinct patches, similar to what is expected from observations (Fig. 11b, note the upper and lower patches, separated at approximately 1500 m depth).

In summary, for all models, we find strong positive correlations between at least part of the inflow and the biases in properties in the deep Arctic. The volume fluxes are biased low in most models, which coupled with the fact that Fram Strait is biased warm results in seemingly accurate heat fluxes through Fram Strait. Nevertheless, it would be desirable to understand why the volume fluxes are inaccurate. In observations, heat and volume fluxes have their largest values in winter, typically February/March, and lowest values in spring/summer, typically June (Schauer et al. 2004; Beszczynska-Möller et al. 2012; De Steur et al. 2014). In our models, the majority follow this pattern of maximum in winter and minimum in summer, although the maximum can be found in any month. The exceptions are GISS-E2-1-H and NorESM2-LM, who have their lowest values in winter for both heat (Fig. 10c) and volume (Fig. 10d). The yearly range can be large in some models (up to 32.4 TW for the heat inflow in MIROC6, and 2.3 Sv for the volume inflow in GFDL-CM4), but so can it in observations (10-50 TW and 4-6 Sv Schauer et al. 2004; Beszczynska-Möller et al. 2012; De Steur et al. 2014).

The reason why the fluxes through Fram Strait are highest in winter can be found in the processes that cause them. In models (Årthun and Eldevik 2016; Muilwijk et al. 2019) as in observations (Wang et al. 2020), regardless of the depth level considered (von Appen et al. 2015; Chatterjee et al. 2018), the heat and volume fluxes through Fram Strait are driven at least in part by the gyre and/or winter convective activity in the Nordic Seas (Smedsrud et al. 2022). The convective activity values in CMIP6 models were recently published by Heuzé (2021): they showed that all the models that we consider here largely overestimate it. In particular, all models but CAMS-CSM1-0 had mixed layers deeper than 1000 m every year over 1985-2014 over an extensive region, which is visible on supp. Fig. A3; CAMS-CSM1-0 did so only 24 out of 30 years. Comparing our fluxes with their mean deep mixed volume, i.e. sum of the cell area multiplied by the mixed layer depth (MLD) for all cells where that MLD is deeper than 1000 m, we find significant across-model correlations (at 90%) with the heat inflow through Fram Strait (0.48) and the volume outflow (0.42). That is, as in observations, a stronger convective activity in the Nordic Seas is associated with a stronger heat inflow into the Arctic, but also with a stronger volume outflow from the Arctic. These results do not prove causality but suggest a possible chain of biases:

1. The Nordic Seas have biased properties and a biased representation of convective activity (Heuzé 2021);

2. The stronger the volume flux out of the Arctic, the stronger the convective activity in the Nordic Seas;

3. The stronger the convective activity, the stronger the volume transport northward, through Fram Strait and into the Arctic;

4. That volume transport advects the biases in properties from the Nordic Seas to Fram Strait, so that the stronger the volume transport, the more Fram Strait is biased warm. Another possibility is that the convective activity directly sets the properties of the advected water, as has been found in observations before (Langehaug and Falck 2012);

5. The stronger the warm bias, the stronger the heat flux into the Arctic.

This would explain why the "worst" models for the heat fluxes are the "least bad" for the volume fluxes.

4. Discussion and conclusions

In this study, we first quantified biases in the Atlantic Water in all deep basins of the Arctic. In agreement with Khosravi et al. (2022), we find that its core is too cold by 0.4°C on average, too deep by 400 m, and in half of the models the Atlantic layer extends all the way to the seafloor, i.e. the properties do not evolve with depth as they do in the real ocean. CMIP5 models were found to somewhat correctly reproduce the cooling and deepening of the Atlantic Water core as the water travels away from Fram Strait (Shu et al. 2019). In CMIP6, our results show the opposite, that in most models the properties do not change from basin to basin. The circulation was not further investigated in CMIP5, so we cannot say which modelling change made the result worse; in CMIP6, we here attribute it to a lack of shelf overflows in most models, a result previously found in ocean-only simulations (Ilıcak et al. 2016), and an inaccurate flow through Fram Strait. To the best of our knowledge, no study was performed on CMIP5 models to quantify biases in deep and bottom water properties in the Arctic; we here determine that they are too warm by more than 1°C as multi-model average. Our findings reveal a strong decoupling between the upper layer and the rest of the deep Arctic (below 200 m), which is quite homogeneous in depth and between the basins.

We linked these biases to processes both within and out of the Arctic. Within the Arctic, the main issue is the absence of ventilation: only three models appear to have dense water overflows, and these are taking place at only two locations (compare e.g. to the list in Luneva et al. 2020), and do not seem to ventilate the deepest layers. Our results are limited by the fact that too few models provide the age of water output, and that a monthly resolution may be too coarse to effectively track overflows as they cascade off the shelf. Nevertheless, this finding comes as no surprise considering that the models suffer from the same overflow-issue in the rest of the world (Heuzé 2021), but this issue is particularly acute in the Arctic where no other process can replace overflows (Peralta-Ferriz and Woodgate 2015), and where open ocean deep mixing is rather indicative of inaccurate stratification (Lique and Thomas 2018). The higher resolution of CMIP6 models compared to CMIP5 was not enough to improve the overflows; in fact, it seems unlikely that such processes can ever become explicitly represented in global climate models (Fox-Kemper et al. 2019). Instead, one can notice that the three models that seem to have overflows also have isopycnal or terrain-following grids (Table 1). Another solution could be the widespread implementation of overflow parameterisations (e.g. Danabasoglu et al. 2010).

The biases are also related to the circulation: within the Arctic, the age of the oldest waters in the CMIP6 models studied here ranges from 122 to 1946 years (Fig. 7). Despite the models following different protocols for the age calculation, we could attribute the age difference not primarily to different flow velocities, but rather to more coherent flows. The highest resolution model had the most coherent and detailed flow, probably thanks to its eddy-permitting resolution and accurate representation of bathymetry, as discussed above. At Fram Strait, we found that all models underestimate the volume fluxes in and out of the Arctic, i.e. all models are biased slow. The heat flux however appears accurate or even biased high, as the low volume fluxes are compensated by warm temperature biases at Fram Strait. We found across-model relationships between Fram Strait biases and fluxes, and inaccurate properties and deep convective activity in the Nordic Seas: as in observations (e.g. Langehaug and Falck 2012), deep convection is enhanced by the deep outflow from the Arctic and enhances the deep inflow, but also modifies the properties of the water advected through Fram Strait. The inaccurate Nordic Seas convective activity was previously blamed on inaccurate sea ice (Heuzé 2021) and atmospheric (Heuzé 2017) representations, suggesting that detecting the cause for biases in the individual components, for example via SIMIP (Notz et al. 2016) or AMIP (Eyring et al. 2016), may be a necessary first step towards accurately modelling the coupled Arctic system.

Higher resolution, parameterisations and dedicated MIPs can however only go so far when there are virtually no observations to constrain the models. In the database UDASH (Behrendt et al. 2018), there are fewer than 700 full-depth hydrographic profiles in the entire Arctic north of 82°N, and only 40 of them are in winter. Consequently in their recent review, Solomon et al. (2021) did not even try to investigate the deep Arctic Ocean as there were too few observations; even for the upper ocean, they could not close the freshwater budget as Arctic river discharge timeseries were few and poor. There is an urgent need for more multi-disciplinary and multi-scale (both in time and space) observation campaigns, similar to the recently completed MOSAiC expedition (Rabe et al. 2022), across the entire Arctic, or at least for more coordination and cooperation between different expeditions to properly investigate processes and their interaction, instead of the traditional local component-specific studies.

Acknowledgments. This work was funded via Vetenskapsrådet grant 2018-03859 awarded to Céline Heuzé. Morven Muilwijk received funding from the European Union's Horizon 2020 research and innovation programme under grant agreement No 101003826 via project CRiceS. We acknowledge the World Climate Research Programme, which, through its Working Group on Coupled Modelling, coordinated and promoted CMIP6. We thank the climate modeling groups for producing and making available their model output, the Earth System Grid Federation (ESGF) for archiving the data and providing access, and the multiple funding agencies who support CMIP6 and ESGF. We are grateful to Jianglong Li (BCC-CSM2-MR), Xinyao Rong (CAMS-CSM1-0), Gary Strand (CESM2), Andrew Shao and Neil Swart (CanESM5), Thomas Reerink (EC-Earth3), the GFDL Climate Model Info Team (GFDL-CM4 and -ESM4), Gavin Schmidt (GISS-E2-1-H), Olivier Boucher (IPSL-CM6A-LR), Hiroaki Tatebe and Yoshiki Komuro (MIROC6), Johann Jungclaus (MPI-ESM1-2-HR), Shogo Urakawa (MRI-ESM2-0), Øyvind Seland and Mats Bentsen (NorESM2-LM), and Andrew Yool and Colin Jones (UK-ESM1-0-LL), for their prompt replies to our questions regarding their respective models, indicated in parentheses.

Data availability statement. All CMIP6 data are freely available via the Earth Grid System Federation. For this paper, we used the German Climate Computing Centre (DKRZ) node: `https://esgf-data.dkrz.de/search/cmip6-dkrz/` and the Geophysical Fluid Dynamics Laboratory (GFDL) node: `https://esgdata.gfdl.noaa.gov/search/cmip6-gfdl/`.

The Unified Database for Arctic and Subarctic Hydrography is freely available via `https://doi.pangaea.de/10.1594/PANGAEA.872931`. All versions of the World Ocean Atlas climatology are freely available via `https://www.ncei.noaa.gov/products/world-ocean-atlas`. All versions of the Polar science center Hydrographic Climatology are freely available via `http://psc.apl.washington.edu/nonwp_projects/PHC/Climatology.html`. The EN4 climatology is freely available via `https://www.metoffice.gov.uk/hadobs/en4/`. The gridded bathymetry GEBCO is freely available via `https://www.gebco.net/data_and_products/gridded_bathymetry_data/`.

The volume, heat, and salt flux time series will be submitted to PANGAEA during the peer-review process; we will add their DOI here latest during copy-editing.

APPENDIX

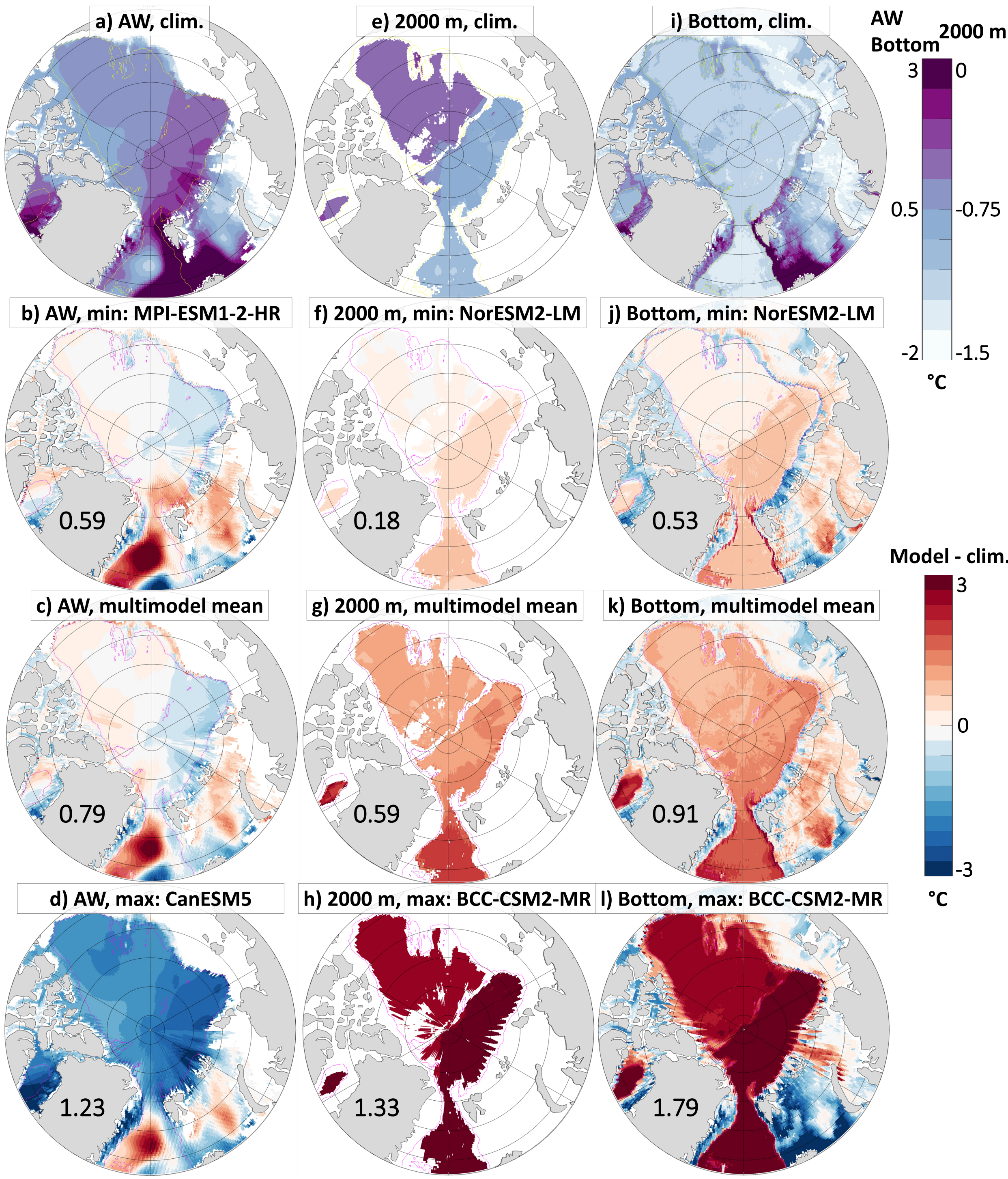

FIG. A1. Potential temperature in the WOA18 climatology (top row) and bias when compared to this climatology for the least biased model (second row), the multimodel mean (third row) and the most biased model (last row), for the Atlantic Water core (first column), 2000 m depth (second column), and the bottom (last column). The numbers are the respective Pan-Arctic area-weighted root mean square errors. See Fig. 4 and supp. Fig. A2 for the density and salinity.

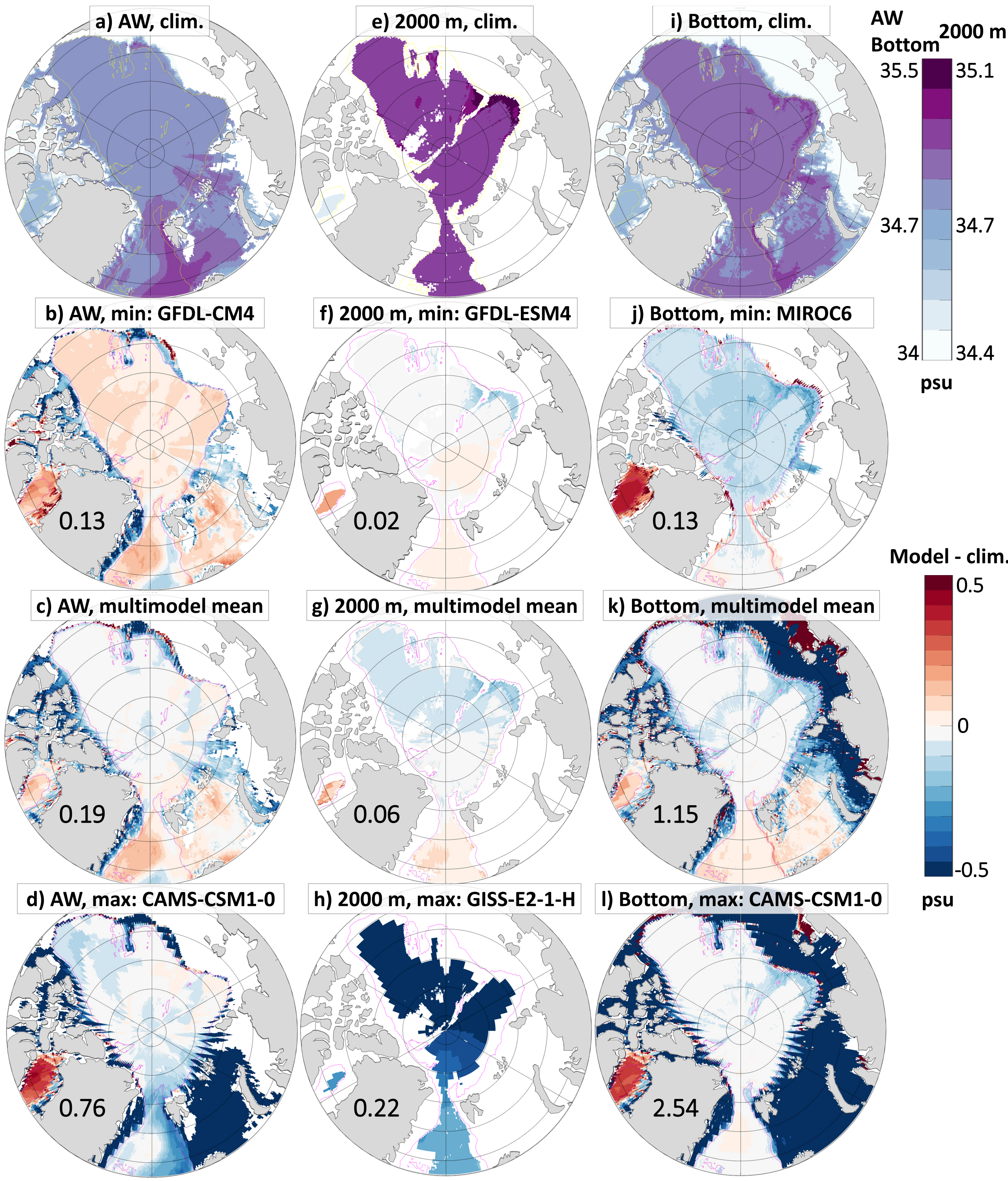

FIG. A2. Salinity in the WOA18 climatology (top row) and bias when compared to this climatology for the least biased model (second row), the multimodel mean (third row) and the most biased model (last row), for the Atlantic Water core (first column), 2000 m depth (second column), and the bottom (last column). The numbers are the respective Pan-Arctic area-weighted root mean square errors. See Fig. 4 and supp. Fig. A1 for the density and temperature.

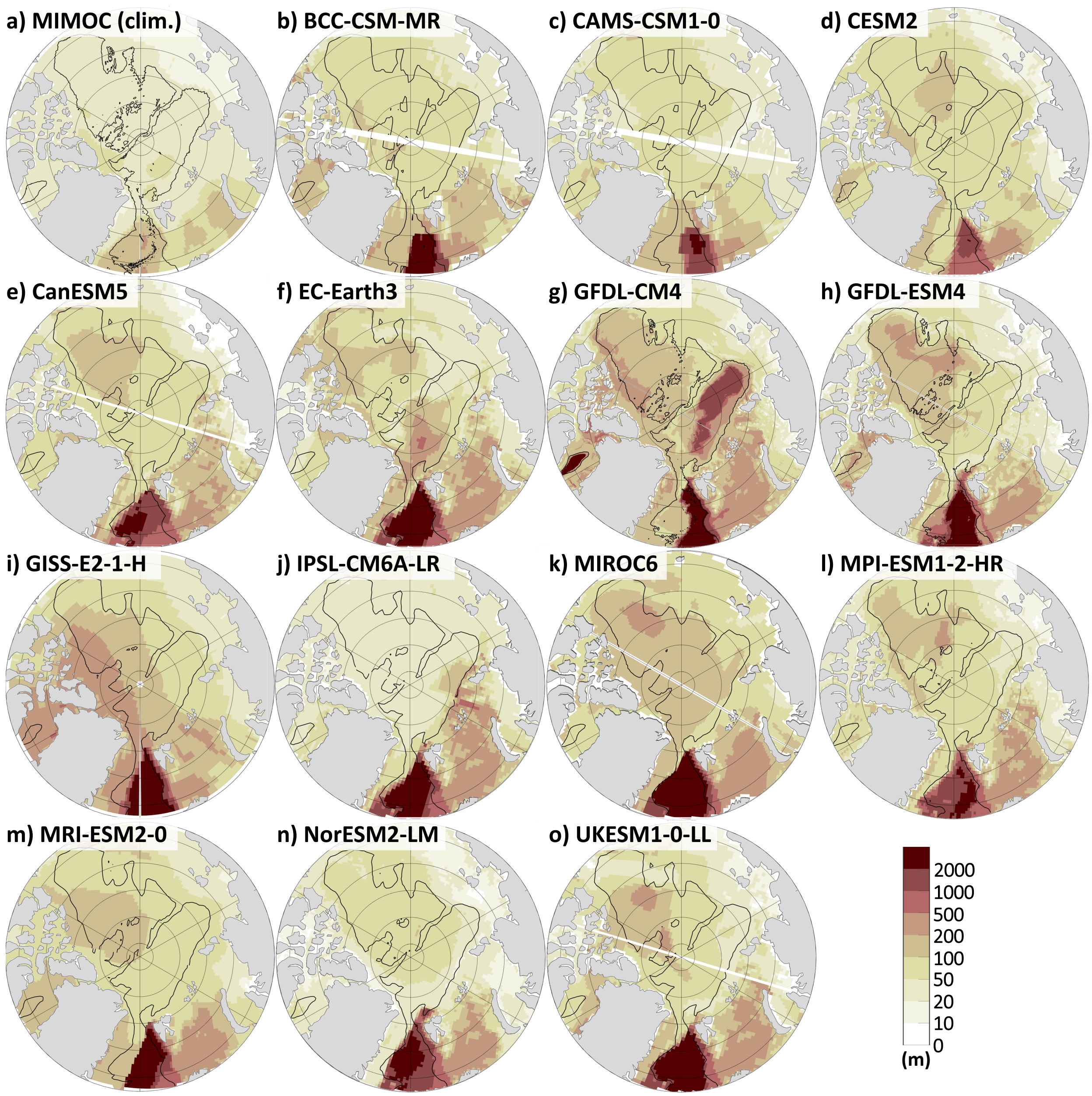

FIG. A3. a) Maximum of the monthly climatological mean mixed layer depth (MLD) from MIMOC (Schmidtko et al. 2013); b)-o) Maximum mixed layer depth over the period January 1985 - December 2014 for each CMIP6 model. Note the logarithmic colour scale. On each panel, the black contour is the 2000 m isobath from a) GEBCO and b)-o) the individual models.

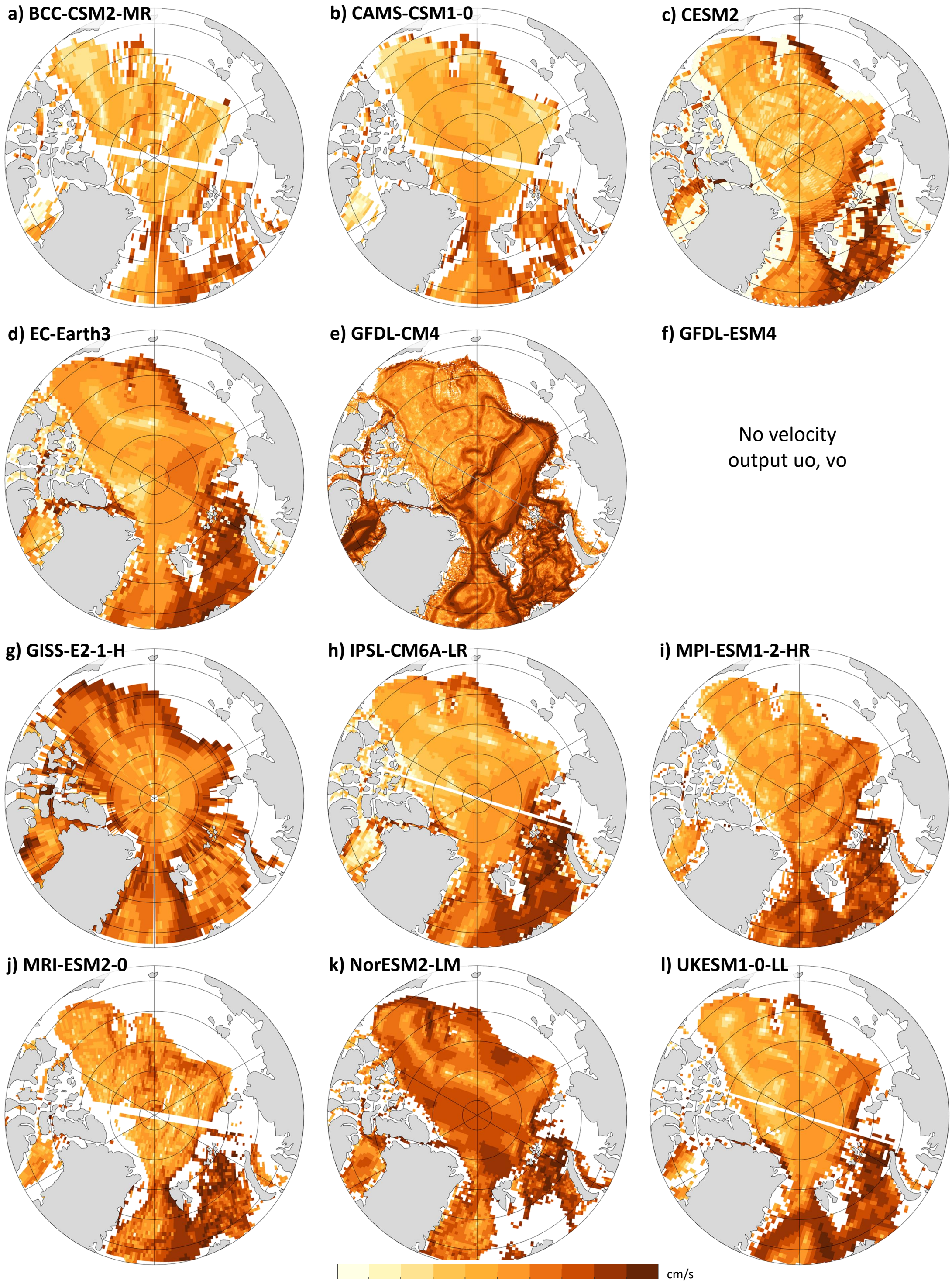

FIG. A4. Velocity of the Atlantic Water core for the models not shown on Fig. 8. Note the logarithmic scale.

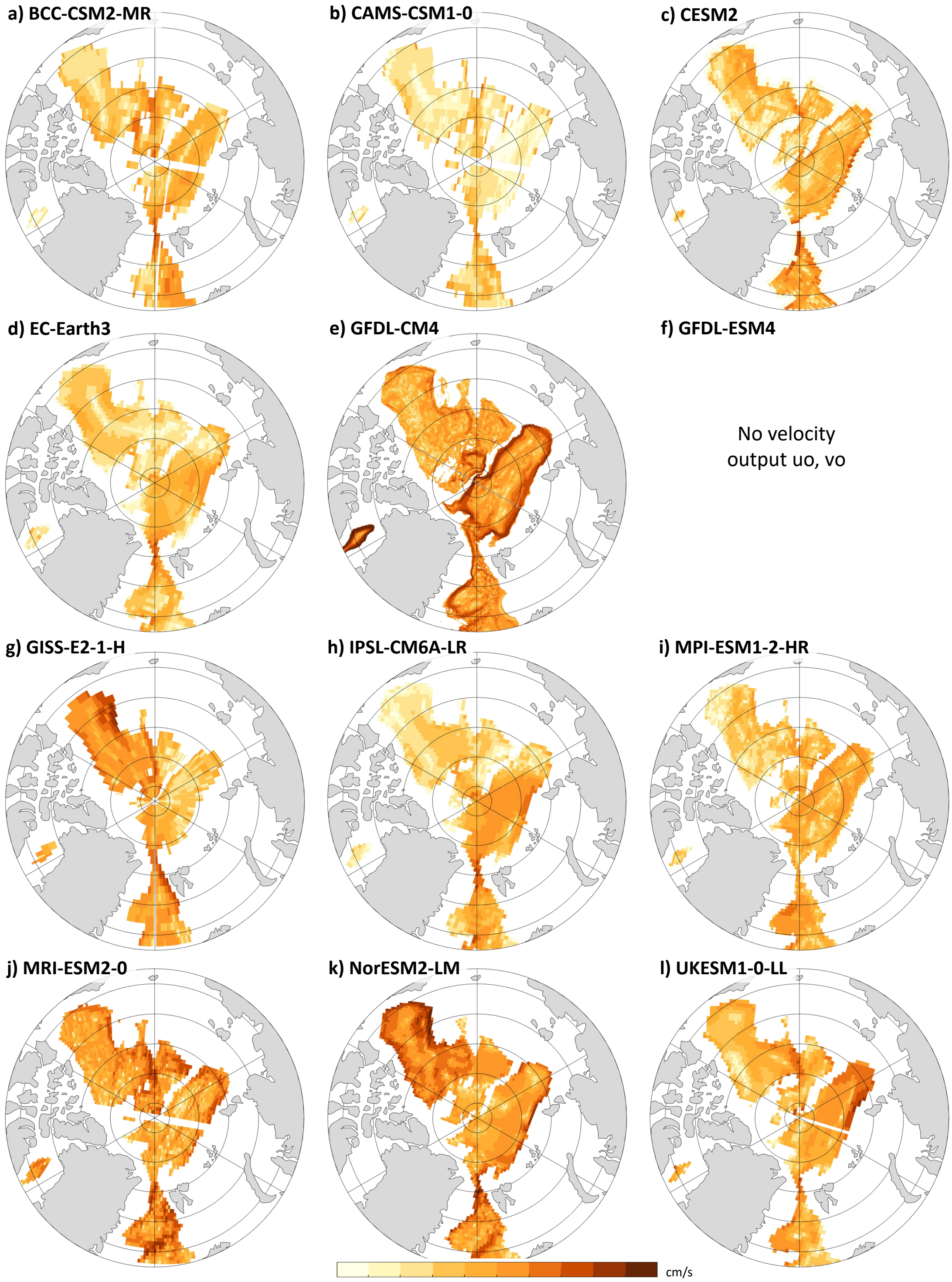

Fig. A5. Velocity at 2000 m depth for the models not shown on Fig. 8. Note the logarithmic scale.

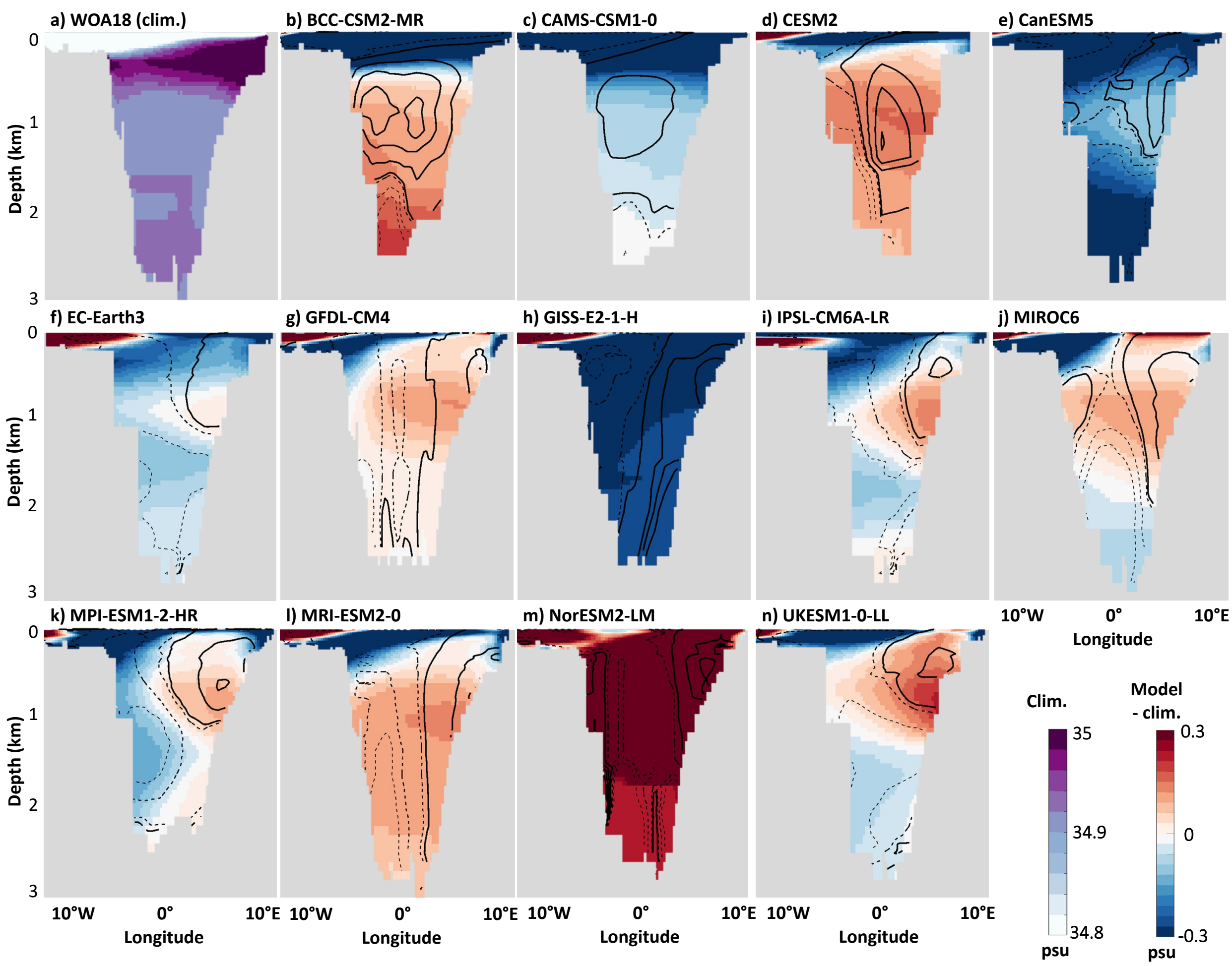

FIG. A6. a) Salinity across Fram Strait in WOA18; b)-n) difference between each model's salinity and that of WOA18 across Fram Strait (shading), along with their volume flux as black lines (0.02 Sv contours; plain means positive, into the Arctic; dashed negative, out of the Arctic). Temperature biases are on Fig. 9

TABLE A1. Area-weighted mean bias model minus WOA18 climatology in potential temperature (first line, left), salinity (first line, right; unit: psu), depth (second line, left) and density σ_2 (second line, right; unit: kg m^{-3}) of the Atlantic Water core for each model and the multi-model mean "MMM" in the four deep basins and on the two shelf regions of interest.

Model	Nansen	Amundsen	Makarov	Canada	Sib. Shelf	Gre. Shelf
BCC-CSM2-MR	0.27 °C; 0.22	0.72 °C; 0.27	1.12 °C; 0.31	1.27 °C; 0.35	-0.52 °C; -0.39	-0.74 °C; -0.63
	1321 m; σ= 0.14	1374 m; σ= 0.12	1332 m; σ= 0.1	1255 m; σ= 0.11	57 m; σ= -0.24	42 m; σ= -0.42
CAMS-CSM1-0	-0.03 °C; -0.07	0.38 °C; -0.04	0.75 °C; -0.02	0.81 °C; -0.05	-0.29 °C; -0.53	0.39 °C; -0.56
	368 m; σ= -0.05	376 m; σ= -0.08	363 m; σ= -0.11	206 m; σ= -0.14	44 m; σ= -0.37	33 m; σ= -0.51
CESM2	0.11 °C; 0.11	0.39 °C; 0.12	0.77 °C; 0.14	0.93 °C; 0.16	0.28 °C; 0.01	1.05 °C; 0.11
	515 m; σ= 0.08	726 m; σ= 0.04	792 m; σ= 0.01	571 m; σ= 0.01	39 m; σ= -0.02	90 m; σ= -0.06
CanESM5	-2.31 °C; -0.26	-2.12 °C; -0.25	-1.78 °C; -0.26	-1.68 °C; -0.26	-0.34 °C; -0.10	-1.67 °C; -0.46
	591 m; σ= 0.07	1020 m; σ= 0.04	999 m; σ= -0.01	979 m; σ= -0.02	28 m; σ= -0.04	45 m; σ= -0.17
EC-Earth3	-1.13 °C; -0.12	-0.65 °C; -0.14	-0.06 °C; -0.12	0.24 °C; -0.09	0.04 °C; -0.02	-0.9 °C; -0.10
	390 m; σ= 0.05	178 m; σ= -0.03	349 m; σ= -0.09	322 m; σ= -0.10	14 m; σ= -0.02	50 m; σ= 0.03
GFDL-CM4	-0.29 °C; 0.04	0.03 °C; 0.04	0.31 °C; 0.04	0.35 °C; 0.05	-0.05 °C; -0.01	-0.08 °C; -0.11
	370 m; σ= 0.07	371 m; σ= 0.03	388 m; σ= 0.00	502 m; σ= 0.00	8 m; σ= 0.00	26 m; σ= -0.08
GFDL-ESM4	-0.59 °C; 0.12	-0.59 °C; 0.10	-0.43 °C; 0.12	-0.40 °C; 0.10	0.04 °C; 0.03	0.19 °C; -0.01
	256 m; σ= 0.17	337 m; σ= 0.16	655 m; σ= 0.15	408 m; σ= 0.12	14 m; σ= 0.02	48 m; σ= -0.03
GISS-E2-1-H	-1.55 °C; -0.58	-1.07 °C; -0.57	-0.82 °C; -0.66	-0.75 °C; -0.72	-0.37 °C; -0.33	-1.21 °C; -0.54
	399 m; σ= -0.27	416 m; σ= -0.32	280 m; σ= -0.42	63 m; σ= -0.48	21 m; σ= -0.21	66 m; σ= -0.28
IPSL-CM6A-LR	-0.80 °C; -0.05	-0.56 °C; -0.07	-0.26 °C; -0.08	-0.22 °C; -0.09	0.34 °C; -0.02	-0.77 °C; -0.09
	477 m; σ= 0.06	467 m; σ= 0.01	681 m; σ= -0.03	574 m; σ= -0.04	28 m; σ= -0.06	67 m; σ= 0.03
MIROC6	0.05 °C; 0.00	0.09 °C; -0.02	0.27 °C; -0.03	0.25 °C; -0.02	0.01 °C; -0.05	1 °C; -0.08
	338 m; σ= -0.01	390 m; σ= -0.03	473 m; σ= -0.05	517 m; σ= -0.04	20 m; σ= -0.04	135 m; σ= -0.21
MPI-ESM1-2-HR	-0.11 °C; -0.07	-0.32 °C; -0.11	-0.18 °C; -0.13	-0.08 °C; -0.09	0.04 °C; -0.09	-0.28 °C; -0.27
	213 m; σ= -0.04	271 m; σ= -0.05	448 m; σ= -0.08	507 m; σ= -0.06	19 m; σ= -0.08	33 m; σ= -0.17
MRI-ESM2-0	0.13 °C; 0.06	0.51 °C; 0.06	0.86 °C; 0.06	0.98 °C; 0.07	0.27 °C; -0.01	0.62 °C; 0.00
	756 m; σ= 0.03	891 m; σ= -0.01	1029 m; σ= -0.06	868 m; σ= -0.07	54 m; σ= -0.04	209 m; σ= -0.08
NorESM2-LM	-1.78 °C; 0.18	-1.46 °C; 0.18	-1.06 °C; 0.19	-0.93 °C; 0.21	-0.14 °C; 0.14	-0.54 °C; 0.06
	77 m; σ= 0.36	116 m; σ= 0.31	123 m; σ= 0.28	3 m; σ= 0.27	7 m; σ= 0.13	1 m; σ= 0.12
UKESM1-0-LL	-1.93 °C; -0.04	-1.78 °C; -0.05	-1.43 °C; -0.06	-1.28 °C; -0.05	-0.21 °C; 0.01	-1.02 °C; -0.07
	589 m; σ= 0.20	702 m; σ= 0.17	645 m; σ= 0.11	454 m; σ= 0.11	21 m; σ= 0.04	36 m; σ= 0.06
MMM	-0.44 °C; -0.02	-0.44 °C; -0.03	-0.12 °C; -0.02	0.08 °C; -0.03	-0.02 °C; -0.02	-0.41 °C; -0.09
	395 m; σ = 0.06	403 m; σ = 0.02	559 m; σ = -0.02	504 m; σ = -0.03	21 m; σ = -0.04	46 m; σ = -0.08

TABLE A2. Area-weighted mean bias model minus WOA18 climatology in potential temperature (first line, left), salinity (first line, right; unit: psu) and density σ_2 (second line) of the Arctic deep water, defined here as properties at 2000 m depth, for each model and the multi-model mean "MMM" in the four deep basins.

Model	Nansen	Amundsen	Makarov	Canada
BCC-CSM2-MR	2.50 °C; 0.19 -0.15 kg m^{-3}	2.75 °C; 0.21 -0.17 kg m^{-3}	2.17 °C; 0.18 -0.12 kg m^{-3}	2.31 °C; 0.22 -0.10 kg m^{-3}
CAMS-CSM1-0	1.57 °C; -0.02 -0.19 kg m^{-3}	1.72 °C; -0.03 -0.22 kg m^{-3}	1.28 °C; -0.04 -0.18 kg m^{-3}	1.35 °C; -0.03 -0.18 kg m^{-3}
CESM2	2.20 °C; 0.07 -0.20 kg m^{-3}	2.27 °C; 0.06 -0.22 kg m^{-3}	1.83 °C; 0.04 -0.19 kg m^{-3}	1.83 °C; 0.05 -0.18 kg m^{-3}
CanESM5	-0.04 °C; -0.28 -0.22 kg m^{-3}	-0.12 °C; -0.30 -0.23 kg m^{-3}	-0.38 °C; -0.31 -0.20 kg m^{-3}	-0.51 °C; -0.35 -0.22 kg m^{-3}
EC-Earth3	1.16 °C; -0.07 -0.18 kg m^{-3}	1.14 °C; -0.09 -0.20 kg m^{-3}	0.86 °C; -0.09 -0.17 kg m^{-3}	0.88 °C; -0.09 -0.17 kg m^{-3}
GFDL-CM4	0.86 °C; 0.00 -0.10 kg m^{-3}	0.82 °C; -0.02 -0.10 kg m^{-3}	0.90 °C; -0.04 -0.13 kg m^{-3}	0.92 °C; -0.04 -0.13 kg m^{-3}
GFDL-ESM4	1.13 °C; 0.13 -0.02 kg m^{-3}	1.13 °C; 0.12 -0.03 kg m^{-3}	0.75 °C; 0.06 -0.04 kg m^{-3}	0.50 °C; 0.03 -0.03 kg m^{-3}
GISS-E2-1-H	0.28 °C; -0.29 -0.26 kg m^{-3}	0.29 °C; -0.42 -0.37 kg m^{-3}	-0.45 °C; -0.41 -0.28 kg m^{-3}	-0.72 °C; -0.47 -0.30 kg m^{-3}
IPSL-CM6A-LR	1.23 °C; -0.09 -0.21 kg m^{-3}	1.21 °C; -0.11 -0.22 kg m^{-3}	0.88 °C; -0.13 -0.20 kg m^{-3}	0.87 °C; -0.13 -0.20 kg m^{-3}
MIROC6	1.32 °C; -0.08 -0.21 kg m^{-3}	1.30 °C; -0.09 -0.22 kg m^{-3}	1.08 °C; -0.11 -0.21 kg m^{-3}	1.11 °C; -0.09 -0.20 kg m^{-3}
MPI-ESM1-2-HR	1.09 °C; -0.13 -0.22 kg m^{-3}	0.99 °C; -0.16 -0.24 kg m^{-3}	0.74 °C; -0.15 -0.20 kg m^{-3}	0.89 °C; -0.15 -0.22 kg m^{-3}
MRI-ESM2-0	2.45 °C; 0.01 -0.28 kg m^{-3}	2.45 °C; -0.01 -0.29 kg m^{-3}	2.13 °C; -0.03 -0.28 kg m^{-3}	2.13 °C; -0.04 -0.29 kg m^{-3}
NorESM2-LM	0.39 °C; 0.20 0.12 kg m^{-3}	0.33 °C; 0.19 0.12 kg m^{-3}	0.07 °C; 0.16 0.12 kg m^{-3}	0.00 °C; 0.17 0.14 kg m^{-3}
UKESM1-0-LL	0.22 °C; -0.09 -0.10 kg m^{-3}	0.15 °C; -0.11 -0.10 kg m^{-3}	-0.10 °C; -0.14 -0.10 kg m^{-3}	-0.14 °C; -0.15 -0.10 kg m^{-3}
MMM	1.14 °C; -0.04 -0.20 kg m^{-3}	1.14 °C; -0.06 -0.22 kg m^{-3}	0.87 °C; -0.07 -0.18 kg m^{-3}	0.89 °C; -0.07 -0.18 kg m^{-3}

TABLE A3. Area-weighted mean bias model minus WOA18 climatology in potential temperature (first line, left), salinity (first line, right; unit: psu), and density σ_2 (second line) of the bottom water, defined as the deepest grid cell with values, for each model and the multi-model mean "MMM" in the four deep basins and on the two shelf regions of interest.

Model	Nansen	Amundsen	Makarov	Canada	Sib. Shelf	Gre. Shelf
BCC-CSM2-MR	2.88 °C; 0.18 -0.20 kg m^{-3}	2.91 °C; 0.21 -0.18 kg m^{-3}	2.55 °C; 0.21 -0.14 kg m^{-3}	2.46 °C; 0.23 -0.12 kg m^{-3}	-0.47 °C; -1.79 -1.37 kg m^{-3}	-0.62 °C; -0.70 -0.49 kg m^{-3}
CAMS-CSM1-0	1.63 °C; -0.05 -0.22 kg m^{-3}	1.52 °C; -0.03 -0.19 kg m^{-3}	1.39 °C; -0.05 -0.19 kg m^{-3}	1.26 °C; -0.03 -0.17 kg m^{-3}	-0.06 °C; -3.07 -2.42 kg m^{-3}	0.53 °C; -0.89 -0.79 kg m^{-3}
CESM2	2.24 °C; 0.05 -0.22 kg m^{-3}	2.14 °C; 0.05 -0.21 kg m^{-3}	2.00 °C; 0.04 -0.21 kg m^{-3}	1.62 °C; 0.04 -0.16 kg m^{-3}	0.39 °C; 0.02 -0.06 kg m^{-3}	1.34 °C; 0.16 -0.05 kg m^{-3}
CanESM5	-0.19 °C; -0.25 -0.18 kg m^{-3}	-0.25 °C; -0.24 -0.17 kg m^{-3}	-0.42 °C; -0.34 -0.22 kg m^{-3}	-0.66 °C; -0.26 -0.14 kg m^{-3}	-0.31 °C; -0.93 -0.73 kg m^{-3}	-1.52 °C; -0.51 -0.24 kg m^{-3}
EC-Earth3	1.30 °C; -0.04 -0.17 kg m^{-3}	1.31 °C; -0.04 -0.17 kg m^{-3}	1.04 °C; -0.07 -0.17 kg m^{-3}	0.86 °C; -0.02 -0.11 kg m^{-3}	0.30 °C; 0.51 0.36 kg m^{-3}	-0.72 °C; -0.05 0.04 kg m^{-3}
GFDL-CM4	0.59 °C; -0.02 -0.08 kg m^{-3}	0.50 °C; -0.02 -0.07 kg m^{-3}	0.74 °C; -0.04 -0.11 kg m^{-3}	0.49 °C; -0.02 -0.07 kg m^{-3}	0.04 °C; -0.83 -0.68 kg m^{-3}	0.13 °C; -0.11 -0.11 kg m^{-3}
GFDL-ESM4	1.27 °C; 0.11 -0.05 kg m^{-3}	1.24 °C; 0.11 -0.05 kg m^{-3}	0.87 °C; 0.07 -0.04 kg m^{-3}	0.57 °C; 0.03 -0.04 kg m^{-3}	0.18 °C; -1.24 -1.01 kg m^{-3}	0.35 °C; -0.02 -0.07 kg m^{-3}
GISS-E2-1-H	0.08 °C; -0.20 -0.16 kg m^{-3}	0.07 °C; -0.37 -0.30 kg m^{-3}	-0.52 °C; -0.40 -0.26 kg m^{-3}	-0.83 °C; -0.43 -0.26 kg m^{-3}	-0.17 °C; -0.24 -0.17 kg m^{-3}	-1.01 °C; -0.39 -0.19 kg m^{-3}
IPSL-CM6A-LR	1.29 °C; -0.02 -0.16 kg m^{-3}	1.28 °C; -0.03 -0.16 kg m^{-3}	1.03 °C; -0.07 -0.17 kg m^{-3}	0.89 °C; -0.03 -0.13 kg m^{-3}	0.75 °C; 0.36 0.18 kg m^{-3}	-0.52 °C; -0.05 0.03 kg m^{-3}
MIROC6	1.22 °C; -0.11 -0.22 kg m^{-3}	1.18 °C; -0.11 -0.22 kg m^{-3}	1.04 °C; -0.12 -0.21 kg m^{-3}	1.14 °C; -0.10 -0.21 kg m^{-3}	0.08 °C; 0.00 -0.01 kg m^{-3}	1.22 °C; 0.10 -0.10 kg m^{-3}
MPI-ESM1-2-HR	1.18 °C; -0.17 -0.26 kg m^{-3}	1.01 °C; -0.20 -0.26 kg m^{-3}	0.92 °C; -0.19 -0.25 kg m^{-3}	0.96 °C; -0.17 -0.24 kg m^{-3}	0.09 °C; -1.34 -1.09 kg m^{-3}	-0.14 °C; -0.37 -0.28 kg m^{-3}
MRI-ESM2-0	2.39 °C; -0.05 -0.31 kg m^{-3}	2.33 °C; -0.05 -0.31 kg m^{-3}	2.20 °C; -0.04 -0.30 kg m^{-3}	2.10 °C; -0.05 -0.29 kg m^{-3}	0.45 °C; 0.31 0.18 kg m^{-3}	0.53 °C; -0.06 -0.11 kg m^{-3}
NorESM2-LM	0.66 °C; 0.41 0.25 kg m^{-3}	0.60 °C; 0.42 0.27 kg m^{-3}	0.12 °C; 0.17 0.12 kg m^{-3}	0.02 °C; 0.17 0.13 kg m^{-3}	-0.03 °C; -0.82 -0.66 kg m^{-3}	-0.35 °C; 0.16 0.18 kg m^{-3}
UKESM1-0-LL	0.26 °C; -0.11 -0.12 kg m^{-3}	0.22 °C; -0.12 -0.12 kg m^{-3}	-0.08 °C; -0.15 -0.11 kg m^{-3}	-0.15 °C; -0.16 -0.11 kg m^{-3}	-0.16 °C; -0.31 -0.25 kg m^{-3}	-0.87 °C; -0.06 0.05 kg m^{-3}
MMM	1.25 °C; -0.04 -0.18 kg m^{-3}	1.21 °C; -0.03 -0.18 kg m^{-3}	0.98 °C; -0.06 -0.18 kg m^{-3}	0.88 °C; -0.03 -0.13 kg m^{-3}	0.06 °C; -0.57 -0.45 kg m^{-3}	-0.24 °C; -0.06 -0.10 kg m^{-3}

References

Aagaard, K., 1981: On the deep circulation in the Arctic Ocean. *Deep Sea Research Part A. Oceanographic Research Papers*, **28**, 251–268, https://doi.org/10.1016/0198-0149(81)90066-2.

Aagaard, K., J. Swift, and E. Carmack, 1985: Thermohaline circulation in the Arctic Mediterranean sea. *Journal of Geophysical Research: Oceans*, **90**, 4833–4846, https://doi.org/10.1029/JC090iC03p04833.

Adcroft, A., and Coauthors, 2019: The GFDL global ocean and sea ice model OM4. 0: Model description and simulation features. *Journal of Advances in Modeling Earth Systems*, **11**, 3167–3211, https://doi.org/10.1029/2019MS001726.

Aksenov, Y., V. Ivanov, A. Nurser, S. Bacon, I. Polyakov, A. Coward, A. Naveira-Garabato, and A. Beszczynska-Moeller, 2011: The Arctic circumpolar boundary current. *Journal of Geophysical Research: Oceans*, **116**, https://doi.org/10.1029/2010JC006637.

Årthun, M., and T. Eldevik, 2016: On anomalous ocean heat transport toward the Arctic and associated climate predictability. *Journal of Climate*, **29**, 689–704, https://doi.org/10.1175/JCLI-D-15-0448.1.

Behrendt, A., H. H. Sumata, B. Rabe, and U. Schauer, 2018: UDASH–unified database for Arctic and Subarctic hydrography. *Earth System Science Data*, **10**, 1119–1138, https://doi.org/10.5194/essd-10-1119-2018.

Bernsen, E., H. Dijkstra, and F. Wubs, 2008: A method to reduce the spin-up time of ocean models. *Ocean modelling*, **20**, 380–392, https://doi.org/10.1016/j.ocemod.2007.10.008.

Beszczynska-Möller, A., E. Fahrbach, U. Schauer, and E. Hansen, 2012: Variability in Atlantic water temperature and transport at the entrance to the Arctic Ocean, 1997–2010. *ICES Journal of Marine Science*, **69**, 852–863, https://doi.org/10.1093/icesjms/fss056.

Björk, G., M. Jakobsson, K. Assmann, L. Andersson, J. Nilsson, C. Stranne, and L. Mayer, 2018: Bathymetry and oceanic flow structure at two deep passages crossing the Lomonosov Ridge. *Ocean Science*, **14**, 1–13, https://doi.org/10.5194/os-14-1-2018.

Chatterjee, S., R. Raj, L. Bertino, Ø. Skagseth, M. Ravichandran, and O. Johannessen, 2018: Role of Greenland Sea gyre circulation on Atlantic water temperature variability in the Fram Strait. *Geophysical Research Letters*, **45**, 8399–8406, https://doi.org/10.1029/2018GL079174.

Danabasoglu, G., J. Lamarque, J. Bacmeister, D. A. Bailey, A. K. DuVivier, J. Edwards, and L. K. Emmons et al., 2020: The community earth system model version 2 (CESM2). *Journal of Advances in Modeling Earth Systems*, **12**, https://doi.org/10.1029/2019MS001916.

Danabasoglu, G., W. Large, and B. Briegleb, 2010: Climate impacts of parameterized Nordic Sea overflows. *Journal of Geophysical Research: Oceans*, **115**, https://doi.org/10.1029/2010JC006243.

De Steur, L., E. Hansen, C. Mauritzen, A. Beszczynska-Möller, and E. Fahrbach, 2014: Impact of recirculation on the East Greenland Current in Fram Strait: Results from moored current meter measurements between 1997 and 2009. *Deep Sea Research Part I: Oceanographic Research Papers*, **92**, 26–40, https://doi.org/10.1016/j.dsr.2014.05.018.

Docquier, D., R. Fuentes-Franco, T. Koenigk, and T. Fichefet, 2020: Sea ice—ocean interactions in the barents sea modeled at different resolutions. *Frontiers in Earth Science*, **8**, 172, https://doi.org/10.3389/feart.2020.00172.

Docquier, D., and Coauthors, 2019: Impact of model resolution on arctic sea ice and north atlantic ocean heat transport. *Climate Dynamics*, **53 (7)**, 4989–5017, https://doi.org/10.1007/s00382-019-04840-y.

Döscher, R., M. Acosta, A. Alessandri, P. Anthoni, A. Arneth, T. Arsouze, T. Bergmann, and R. Bernadello et al., 2021: The EC-Earth3 Earth System Model for the Climate Model Intercomparison Project 6. *Geosci. Model Dev. Discuss.*, https://doi.org/10.5194/gmd-2020-446.

Dunne, J., and Coauthors, 2020: The GFDL Earth System Model version 4.1 (GFDL-ESM 4.1): Overall coupled model description and simulation characteristics. *Journal of Advances in Modeling Earth Systems*, https://doi.org/10.1029/2019MS002015.

Environmental Working Group, 1997: Joint US-Russian atlas of the Arctic Ocean for the winter period. National Snow and Ice Data Center.

Environmental Working Group, 1998: Joint US-Russian atlas of the Arctic Ocean for the summer period. National Snow and Ice Data Center.

Eyring, V., S. Bony, G. Meehl, C. Senior, B. Stevens, R. Stouffer, and K. Taylor, 2016: Overview of the Coupled Model Intercomparison Project Phase 6 (CMIP6) experimental design and organization. *Geoscientific Model Development*, **9**, 1937–1958, https://doi.org/10.5194/gmd-9-1937-2016.

Fox-Kemper, B., and Coauthors, 2019: Challenges and prospects in ocean circulation models. *Frontiers in Marine Science*, **6**, 65, https://doi.org/10.3389/fmars.2019.00065.

Frank, M., W. Smethie Jr, and R. Bayer, 1998: Investigation of subsurface water flow along the continental margin of the Eurasian Basin using the transient tracers tritium, 3He, and CFCs. *Journal of Geophysical Research: Oceans*, **103**, 30 773–30 792, https://doi.org/10.1029/1998JC900003.

GEBCO Compilation Group, 2021: GEBCO 2021 Grid. doi:10.5285/c6612cbe-50b3-0cff-e053-6c86abc09f8f.

Good, S. A., M. J. Martin, and N. A. Rayner, 2013: EN4: quality controlled ocean temperature and salinity profiles and monthly objective analyses with uncertainty estimates. *Journal of Geophysical Research: Oceans*, **118**, 6704–6716, https://doi.org/10.1002/2013JC009067.

Griffies, S., and Coauthors, 2016: OMIP contribution to CMIP6: Experimental and diagnostic protocol for the physical component of the Ocean Model Intercomparison Project. *Geoscientific Model Development*, **9**, 3231–3296, https://doi.org/10.5194/gmd-9-3231-2016.

Heuzé, C., 2017: North Atlantic deep water formation and AMOC in CMIP5 models. *Ocean Science*, **13**, 609–622, https://doi.org/10.5194/os-13-609-2017.

Heuzé, C., 2021: Antarctic Bottom Water and North Atlantic Deep Water in CMIP6 models. *Ocean Science*, https://doi.org/10.5194/os-17-59-2021.

Hinrichs, C., Q. Wang, N. Koldunov, L. Mu, T. Semmler, D. Sidorenko, and T. Jung, 2021: Atmospheric wind biases: A challenge for simulating the arctic ocean in coupled models?

Journal of Geophysical Research: Oceans, **126 (10)**, e2021JC017 565, https://doi.org/10.1029/2021JC017565.

Ilıcak, M., and Coauthors, 2016: An assessment of the Arctic Ocean in a suite of interannual CORE-II simulations. Part III: Hydrography and fluxes. *Ocean Modelling*, **100**, 141–161, https://doi.org/10.1016/j.ocemod.2016.02.004.

IPCC, 2019: *IPCC Special Report on the Ocean and Cryosphere in a Changing Climate*. Cambridge University Press.

IPCC, 2021: *Climate Change 2021: The Physical Science Basis. Contribution of Working Group I to the Sixth Assessment Report of the Intergovernmental Panel on Climate Change*. Cambridge University Press.

Ivanov, V., G. Shapiro, J. Huthnance, D. Aleynik, and P. Golovin, 2004: Cascades of dense water around the world ocean. *Progress in oceanography*, **60**, 47–98, https://doi.org/10.1016/j.pocean.2003.12.002.

Karcher, M., F. Kauker, R. Gerdes, E. Hunke, and J. Zhang, 2007: On the dynamics of atlantic water circulation in the arctic ocean. *Journal of Geophysical Research: Oceans*, **112 (C4)**, https://doi.org/10.1029/2006JC003630.

Kelley, M., and Coauthors, 2020: GISS-E2. 1: Configurations and climatology. *Journal of Advances in Modeling Earth Systems*, https://doi.org/10.1029/2019MS002025.

Khosravi, N., Q. Wang, N. Koldunov, C. Hinrichs, T. Semmler, S. Danilov, and T. Jung, 2022: The Arctic Ocean in CMIP6 models: Biases and projected changes in temperature and salinity. *Earth's Future*, e2021EF002282, https://doi.org/10.1029/2021EF002282.

Korhonen, M., B. Rudels, M. Marnela, A. Wisotzki, and J. Zhao, 2013: Time and space variability of freshwater content, heat content and seasonal ice melt in the Arctic Ocean from 1991 to 2011. *Ocean Science*, **9**, 1015–1055, https://doi.org/10.5194/os-9-1015-2013.

Kwok, R., 2018: Arctic sea ice thickness, volume, and multiyear ice coverage: losses and coupled variability (1958–2018). *Environmental Research Letters*, **13**, 105 005, https://doi.org/10.1088/1748-9326/aae3ec.

Langehaug, H., and E. Falck, 2012: Changes in the properties and distribution of the intermediate and deep waters in the Fram Strait. *Progress in Oceanography*, **96**, 57–76, https://doi.org/10.1016/j.pocean.2011.10.002.

Lique, C., and M. Thomas, 2018: Latitudinal shift of the Atlantic Meridional Overturning Circulation source regions under a warming climate. *Nature Climate Change*, **8**, 1013–1020, https://doi.org/10.1038/s41558-018-0316-5.

Locarnini, R., and Coauthors, 2018: *World Ocean Atlas 2018, Volume 1: Temperature*. A. Mishonov Technical Ed.; NOAA Atlas NESDIS 81.

Luneva, M., V. Ivanov, F. Tuzov, Y. Aksenov, J. Harle, S. Kelly, and J. Holt, 2020: Hotspots of dense water cascading in the Arctic Ocean: Implications for the Pacific water pathways. *Journal of Geophysical Research: Oceans*, **125**, e2020JC016 044, https://doi.org/10.1029/2020JC016044.

Lurton, T., and Coauthors, 2020: Implementation of the CMIP6 Forcing Data in the IPSL-CM6A-LR Model. *Journal of Advances in Modeling Earth Systems*, **12**, https://doi.org/10.1029/2019MS001940.

Marnela, M., B. Rudels, I. Goszczko, A. Beszczynska-Möller, and U. Schauer, 2016: Fram Strait and Greenland Sea transports, water masses, and water mass transformations 1999–2010 (and beyond). *Journal of Geophysical Research: Oceans*, **121**, 2314–2346, https://doi.org/10.1002/2015JC011312.

McDougall, T., and P. Barker, 2011: Getting started with TEOS-10 and the Gibbs Seawater (GSW) Oceanographic Toolbox. Tech. rep., OR/IAPSO WG127.

Mignot, J., and Coauthors, 2021: The tuning strategy of IPSL-CM6A-LR. *Journal of Advances in Modeling Earth Systems*, **13**, e2020MS002 340, https://doi.org/10.1029/2020MS002340.

Muilwijk, M., L. Smedsrud, M. Ilıcak, and H. Drange, 2018: Atlantic Water heat transport variability in the 20th century Arctic Ocean from a global ocean model and observations. *Journal of Geophysical Research: Oceans*, **123**, 8159–8179, https://doi.org/10.1029/2018JC014327.

Muilwijk, M., L. Smedsrud, I. Polyakov, A. Nummelin, C. Heuzé, and H. Zanowski, subm.: Divergence in climate model projections of future Arctic Ocean stratification. *Journal of Climate*.

Muilwijk, M., and Coauthors, 2019: Arctic Ocean response to Greenland Sea wind anomalies in a suite of model simulations. *Journal of Geophysical Research: Oceans*, **124**, 6286–6322, https://doi.org/10.1029/2019JC015101.

Müller, W., and Coauthors, 2018: A Higher-resolution Version of the Max Planck Institute Earth System Model (MPI-ESM1. 2-HR). *Journal of Advances in Modeling Earth Systems*, **10**, https://doi.org/10.1029/2017MS001217.

Nansen, F., 1906: Northern waters: Captain Roald Amundsen's oceanographic observations in the Arctic Seas in 1901. With a discussion of the origin of the Bottom-Waters of the Northern Seas (No. 3). In commission by Jacob Dybwad.

Notz, D., A. Jahn, M. Holland, E. Hunke, F. Massonnet, J. Stroeve, B. Tremblay, and M. Vancoppenolle, 2016: The CMIP6 Sea-Ice Model Intercomparison Project (SIMIP): understanding sea ice through climate-model simulations. *Geoscientific Model Development*, **9**, 3427–3446, https://doi.org/10.5194/gmd-9-3427-2016.

Notz, D., and SIMIP Community, 2020: Arctic sea ice in CMIP6. *Geophysical Research Letters*, **47**, e2019GL086 749, https://doi.org/10.1029/2019GL086749.

Onarheim, I., T. Eldevik, L. Smedsrud, and J. Stroeve, 2018: Seasonal and regional manifestation of Arctic sea ice loss. *Journal of Climate*, **31**, 4917–4932, https://doi.org/10.1175/JCLI-D-17-0427.1.

Peralta-Ferriz, C., and R. Woodgate, 2015: Seasonal and interannual variability of pan-Arctic surface mixed layer properties from 1979 to 2012 from hydrographic data, and the dominance of stratification for multiyear mixed layer depth shoaling. *Progress in Oceanography*, **134**, 19–53, https://doi.org/10.1016/j.pocean.2014.12.005.

Pnyushkov, A., I. Polyakov, V. Ivanov, Y. Aksenov, A. Coward, M. Janout, and B. Rabe, 2015: Structure and variability of the boundary current in the eurasian basin of the arctic ocean. *Deep Sea Research Part I: Oceanographic Research Papers*, **101**, 80–97, https://doi.org/10.1016/j.dsr.2015.03.001.

Polyakov, I., and Coauthors, 2017: Greater role for Atlantic inflows on sea-ice loss in the Eurasian Basin of the Arctic Ocean. *Science*, **356**, 285–291, https://doi.org/10.1126/science.aai8204.

Rabe, B., and Coauthors, 2022: Overview of the MOSAiC expedition: Physical oceanography. *Elementa: Science of the Anthropocene*, **10**, 00 062, https://doi.org/10.1525/elementa.2021.00062.

Roberts, M. J., H. T. Hewitt, P. Hyder, D. Ferreira, S. A. Josey, M. Mizielinski, and A. Shelly, 2016: Impact of ocean resolution on coupled air-sea fluxes and large-scale climate. *Geophysical Research Letters*, **43 (19)**, 10–430, https://doi.org/10.1002/2016GL070559.

Rong, X. Y., J. Li, and H. M. Chen, 2019: Introduction of CAMS-CSM model and its participation in CMIP6. *Climate Change Res.*, **6**, https://doi.org/10.12006/j.issn.1673-1719.2019.186.

Rudels, B., 1986: The θ-S relations in the northern seas: Implications for the deep circulation. *Polar Research*, **4**, 133–159, https://doi.org/0.3402/polar.v4i2.6928.

Rudels, B., 2009: *Encyclopedia of ocean sciences, 2nd ed.*, chap. Arctic Ocean circulation. Oxford, UK: Academic Pres.

Rudels, B., G. Björk, R. Muench, and U. Schauer, 1999: Double-diffusive layering in the Eurasian Basin of the Arctic Ocean. *Journal of Marine Systems*, **21**, 3–27, https://doi.org/10.1016/S0924-7963(99)00003-2.

Rudels, B., and D. Quadfasel, 1991: Convection and deep water formation in the Arctic Ocean-Greenland Sea system. *Journal of Marine Systems*, **2**, 435–450, https://doi.org/10.1016/0924-7963(91)90045-V.

Schauer, U., and A. Beszczynska-Möller, 2009: Problems with estimation and interpretation of oceanic heat transport – conceptual remarks for the case of Fram Strait in the Arctic Ocean. *Ocean Science*, **5**, 487–494, https://doi.org/10.5194/os-5-487-2009.

Schauer, U., E. Fahrbach, S. Osterhus, and G. Rohardt, 2004: Arctic warming through the Fram Strait: Oceanic heat transport from 3 years of measurements. *Journal of Geophysical Research: Oceans*, **109**, https://doi.org/10.1029/2003JC001823.

Schlosser, P., and Coauthors, 1997: The first trans-Arctic 14C section: comparison of the mean ages of the deep waters in the Eurasian and Canadian basins of the Arctic Ocean. *Nuclear*

Instruments and Methods in Physics Research Section B: Beam Interactions with Materials and Atoms, **123**, 431–437, https://doi.org/10.1016/S0168-583X(96)00677-5.

Schmidtko, S., G. Johnson, and J. Lyman, 2013: MIMOC: A global monthly isopycnal upper-ocean climatology with mixed layers. *Journal of Geophysical Research: Oceans*, **118**, 1658–1672, https://doi.org/10.1002/jgrc.20122.

Seland, Ø., and Coauthors, 2020: Overview of the Norwegian Earth System Model (NorESM2) and key climate response of CMIP6 DECK, historical, and scenario simulations. *Geoscientific Model Development*, **13**, 6165–6200, https://doi.org/10.5194/gmd-13-6165-2020.

Sellar, A., and Coauthors, 2020: Implementation of UK Earth system models for CMIP6. *Journal of Advances in Modeling Earth Systems*, https://doi.org/10.1029/2019MS001946.

Shu, Q., Q. Wang, J. Su, X. Li, and F. Qiao, 2019: Assessment of the Atlantic water layer in the Arctic Ocean in CMIP5 climate models. *Climate Dynamics*, **53**, 5279–5291, https://doi.org/10.1007/s00382-019-04870-6.

Smedsrud, L., and Coauthors, 2022: Nordic Seas heat loss, Atlantic inflow, and Arctic sea ice cover over the last century. *Reviews of Geophysics*, **60**, e2020RG000 725, https://doi.org/10.1029/2020RG000725.

Smethie, W., D. Chipman, J. Swift, and K. Koltermann, 1988: Chlorofluoromethanes in the Arctic Mediterranean seas: Evidence for formation of bottom water in the Eurasian Basin and deep-water exchange through Fram Strait. *Deep Sea Research Part A Oceanographic Research Papers*, **35**, 347–369, https://doi.org/10.1016/0198-0149(88)90015-5.

Solomon, A., and Coauthors, 2021: Freshwater in the Arctic Ocean 2010–2019. *Ocean Science*, **17**, 1081–1102, https://doi.org/10.5194/os-17-1081-2021.

Steele, M., R. Morley, and W. Ermold, 2001: PHC: A global ocean hydrography with a high-quality Arctic Ocean. *Journal of Climate*, **14**, 2079–2087, https://doi.org/10.1175/1520-0442(2001)014<2079:PAGOHW>2.0.CO;2.

Stouffer, R., A. Weaver, and M. Eby, 2004: A method for obtaining pre-twentieth century initial conditions for use in climate change studies. *Climate Dynamics*, **23**, 327–339, https://doi.org/10.1007/s00382-004-0446-5.

Stroeve, J., and D. Notz, 2018: Changing state of arctic sea ice across all seasons. *Environmental Research Letters*, **13**, 103 001, https://doi.org/10.1088/1748-9326/aade56.

Swart, N., and Coauthors, 2019: The Canadian Earth System Model version 5 (CanESM5. 0.3). *Geoscientific Model Development*, **12**, https://doi.org/10.5194/gmd-2019-177.

Talandier, C., and Coauthors, 2014: Improvements of simulated Western North Atlantic current system and impacts on the AMOC. *Ocean Modelling*, **76**, 1–19, https://doi.org/10.1016/j.ocemod.2013.12.007.

Tanhua, T., E. Jones, E. Jeansson, S. Jutterström, W. S. Jr, D. Wallace, and L. Anderson, 2009: Ventilation of the Arctic Ocean: Mean ages and inventories of anthropogenic CO2 and CFC-11. *Journal of Geophysical Research: Oceans*, **114**, https://doi.org/10.1029/2008JC004868.

Tatebe, H., and Coauthors, 2019: Description and basic evaluation of simulated mean state, internal variability, and climate sensitivity in MIROC6. *Geoscientific Model Development*, **12**, https://doi.org/10.5194/gmd-12-2727-2019.

Timmermans, M., and C. Garrett, 2006: Evolution of the deep water in the Canadian Basin in the Arctic Ocean. *Journal of physical oceanography*, **36**, 866–874, https://doi.org/10.1175/JPO2906.1.

Timmermans, M., P. Winsor, and J. Whitehead, 2005: Deep-water flow over the Lomonosov Ridge in the Arctic Ocean. *Journal of physical oceanography*, **35**, 1489–1493, https://doi.org/10.1175/JPO2765.1.

Valk, O., and Coauthors, 2020: Decrease in 230Th in the Amundsen Basin since 2007: far-field effect of increased scavenging on the shelf? *Ocean Science*, **16**, 221–234, https://doi.org/10.5194/os-16-221-2020.

von Appen, W., U. Schauer, R. Somavilla, E. Bauerfeind, and A. Beszczynska-Möller, 2015: Exchange of warming deep waters across Fram Strait. *Deep Sea Research Part I: Oceanographic Research Papers*, **103**, 86–100, https://doi.org/10.1016/j.dsr.2015.06.003.

Wang, Q., and Coauthors, 2020: Intensification of the Atlantic Water supply to the Arctic Ocean through Fram Strait induced by Arctic sea ice decline. *Geophysical Research Letters*, **47**, e2019GL086 682, https://doi.org/10.1029/2019GL086682.

Woodgate, R., K. Aagaard, R. Muench, J. Gunn, G. Björk, B. Rudels, A. Roach, and U. Schauer, 2001: The Arctic Ocean boundary current along the Eurasian slope and the adjacent Lomonosov Ridge: Water mass properties, transports and transformations from moored instruments. *Deep Sea Research Part I: Oceanographic Research Papers*, **48**, 1757–1792, https://doi.org/10.1016/S0967-0637(00)00091-1.

Wu, T., and Coauthors, 2019: The Beijing Climate Center Climate System Model (BCC-CSM): the main progress from CMIP5 to CMIP6. *Geoscientific Model Development*, **12**, https://doi.org/10.5194/gmd-12-1573-2019.

Yukimoto, S., and Coauthors, 2019: The Meteorological Research Institute Earth System Model version 2.0, MRI-ESM2. 0: Description and basic evaluation of the physical component. *Journal of the Meteorological Society of Japan*, https://doi.org/10.2151/jmsj.2019-051.

Zanowski, H., A. Jahn, and M. Holland, 2021: Arctic Ocean Freshwater in CMIP6 Ensembles: Declining Sea Ice, Increasing Ocean Storage and Export. *Journal of Geophysical Research: Oceans*, **126**, e2020JC016 930, https://doi.org/10.1029/2020JC016930.

Zweng, M., and Coauthors, 2018: *World Ocean Atlas 2018, Volume 2: Salinity*. A. Mishonov Technical Ed.; NOAA Atlas NESDIS 82.